Novel experimental-modeling coupled framework to elucidate the impact of collagen on diaphragm muscle mechanics in Duchenne muscular dystrophy

---

A

Dissertation

Presented to

the faculty of the School of Engineering and Applied Science

University of Virginia

---

in partial fulfillment

of the requirements for the degree

Doctor of Philosophy

by

C. Hunter Wallace

December 2021

APPROVAL SHEET

This

Dissertation

is submitted in partial fulfillment of the requirements
for the degree of

Doctor of Philosophy

Author: C. Hunter Wallace

This Dissertation has been read and approved by the examing committee:

Advisor: Silvia Blemker

Advisor:

Committee Member: Jeffrey Holmes

Committee Member: Shayn Peirce-Cottler

Committee Member: Jason Kerrigan

Committee Member: Glenn Walter

Committee Member:

Committee Member:

Accepted for the School of Engineering and Applied Science:

Jennifer L. West, School of Engineering and Applied Science

December 2021

Novel experimental-modeling coupled framework to elucidate the impact of collagen on diaphragm muscle mechanics in Duchenne muscular dystrophy

By C. Hunter Wallace

Abstract

Duchenne muscular dystrophy is a progressive muscle wasting disease affecting 1 in 3500 boys. It is a recessive X-linked disease caused by a mutation in the dystrophin gene resulting in incomplete translation of the structural protein dystrophin that links the intracellular sarcomere to the extracellular matrix. Despite extensive research, there remains no cure for DMD. Cardiopulmonary failure, understood to be linked to diaphragm dysfunction, is the leading cause of mortality. The lack of this structural protein causes the dystrophic muscle to be highly susceptible to damage, leading to a state of chronic inflammation and replacement of contractile tissue with fibrotic tissue and fat. Understanding how these changes in the constituents of muscle tissue affect the *in vivo* function of the muscle is critical to developing therapies to improve the quality of life for boys with DMD.

The goal of my dissertation is to couple benchtop experiments with computational modeling to elucidate the role of fibrotic tissue in diaphragm dysfunction. To accomplish this, we first measured the biaxial properties of healthy and dystrophic muscle tissue samples before and after enzymatic collagen digestion in order to isolate the effects of collagen on passive tissue mechanics. Our measurements revealed significant correlations between collagen quantity and both along and across fiber stiffness We then measured the *in vivo* mechanics of healthy and dystrophic diaphragms through a novel sonomicrometry method in order to examine how muscular dystrophy impacts the *in vivo* active mechanics. Measurements of *in vivo* diaphragm contraction revealed a significant decrease in strains and strain rates associated with disease state. When considering the effects of fibrosis, we found a significant correlation between collagen quantity and measured strains. Finally, we integrated our experiments to develop and validate finite-element models of the both healthy and dystrophic diaphragms. Using these models, we performed “what-if” simulations to illuminate how restoring either the active or passive mechanics of dystrophic muscle would impact diaphragm function. The modeling analysis predicted a 75% recovery with restoration of the force production capabilities

of healthy muscle and a 35% recovery by changing the passive properties. These results highlight the need to consider both restoration of active properties and the regulation of fibrosis when developing therapies. Further development of the experimental methods and model in this dissertation could provide additional testing metrics for drug therapies as well as identify targets for new therapies.

Contents

List of Figures

List of Equations

Chapter 1

Introduction

1.1 Overview

Skeletal muscle is critical for all aspects of daily life such as locomotion, eating, and breathing. Several neuromuscular diseases, such as Duchenne muscular dystrophy (DMD), that lead to the degeneration of skeletal muscle can severely impact quality of life. Decades of benchtop and modeling research have expanded our understanding of both healthy and pathological muscle; however, there remains no cure for DMD and other neuromuscular diseases. The cause of DMD, incomplete translation of the transmembrane protein dystrophin, is known and the goal is development of therapies that are able to replace this missing protein. Until this is accomplished, we need to develop therapies to improve the quality of life for boys living with DMD today.

To begin to develop therapies targeted towards improving the life of boys with DMD, we must understand the changes that occur to skeletal muscle as a result of the disease. The absence of the dystrophin protein has been shown to make skeletal muscle more susceptible to contraction induced damage.[1,2] This increased susceptibility leads to those everyday movements such as walking, eating, and breathing causing a cycle of degeneration and regeneration thus creating a state of chronic inflammation where healthy muscle tissue is replaced by scar and fat.[3,4] These tissue level changes impact the active and passive mechanics of dystrophic muscle where decreased force production[5–8] and increased stiffness[5,9,10] are both well documented. However, the degree to which these altered active and passive mechanics contribute to the muscle dysfunction is not well understood.

The progressive degeneration of skeletal muscle from everyday use makes the diaphragm muscle, the primary driver of respiration, an important muscle to study in regards to

quality of life for boys with DMD. As boys age and disease progression occurs, they become dependent on respiratory assistive devices and ultimately, respiratory failure is a leading cause of mortality. [11–13] In addition to the clinical need for respiratory assistance, diaphragm dysfunction has been noted through magnetic resonance imaging studies where significantly reduced diaphragm displacements were noted in boys with DMD compared to age-matched controls.[14]

We hypothesize that the fibrosis associated with the state of chronic inflammation in DMD is a primary cause of muscle dysfunction. In fact, collagen digestion has been shown to decrease muscle stiffness[15] but collagen quantity was not found to be correlated with stiffness in mdx mice, a model of DMD, diaphragms.[10] However, these measurements were conducted uniaxially. Whereas, the diaphragm muscle that is fully constrained *in vivo* where properties in multiple directions must be considered. It is our belief that both the along fiber and across fiber properties must be investigated and understood to fully elucidate the impact of fibrosis on the dystrophic diaphragm.

In Chapter 2 of this dissertation, I performed passive biaxial mechanical tests on diaphragm muscle samples from wildtype and *mdx* mice before and after enzymatic digestion of collagen. We predicted that dystrophic muscle would be stiffer than wildtype muscle in both the along and across fiber directions. Furthermore, we predicted that digestion of collagen would decrease the stiffness in both directions. Our measurements revealed significant correlations between collagen quantity and along and across fiber stiffness however collagen quantity alone was not able to account for all measured variability evidenced by low R^2 values (0.12 to 0.17).

In Chapter 3, we developed a method to adapt sonomicrometry for the measurement of both along and across fiber *in vivo* strains of the mouse diaphragm. We predicted that strains in dystrophic mice would be significantly lower than those measured in wildtype mice. Our measurements revealed a significant decrease in strains and strain rates associated with disease state. When considering the effects of fibrosis, we found a significant correlation

between collagen quantity and measured strains; however, similar to the passive mechanics, collagen quantity alone did not account for all of the measured variability (R^2 = 0.26, 0.33). Finally, comparing our passive mechanical data from Chapter 2 to our sonometric measurements, we did not find any significant relationships between the passive stiffness and measured along or across fiber strains.

In Chapter 4, we used the knowledge gained from the experiments in Chapters 2 and 3 to inform a computational model of the mouse diaphragm. Passive biaxial testing data from Chapter 2 were fit to a transversely isotropic, hyperelastic, quasi-incompressible material[16]. Simulations of 6 and 12-month-old wildtype and mdx diaphragm mice were then run and model predictions of along- and across-fiber strains were compared to those measured in Chapter 3. Additionally model predictions of diaphragm amplitude were compared to literature values. Finally, theoretical "what-if" simulations were performed where wildtype parameters were substituted into the dystrophic model to investigate how recovery of active and passive properties affects diaphragm function. We found that restoring the active properties resulted in a 74% recovery and restoring the passive properties a 35% recovery.

Ultimately, we performed a series of experiments that informed a computational model, all investigating the impact of fibrosis on the active and passive mechanics of the dystrophic diaphragm. Our results suggest that collagen has a significant impact on the mechanics but that collagen quantity alone is not able to fully explain the differences measured. Furthermore, we believe that our results demonstrate that while the active properties dominate recovery, the passive properties should also be considered in the development of new therapies for DMD.

1.2 Background

Skeletal muscle structure

Skeletal muscle has a hierarchical structure where contractile elements are surrounded by extracellular matrix (ECM). At the highest level, the epimysium surrounds the entire muscle and

then the perimysium surrounds the muscle fascicles. Within each fascicle, the endomysium surrounds each muscle fiber. Muscle fibers are comprised of the force generating unit of muscle, sarcomeres. The sarcomeres are structurally linked to the ECM through the dystrophin glycoprotein complex.

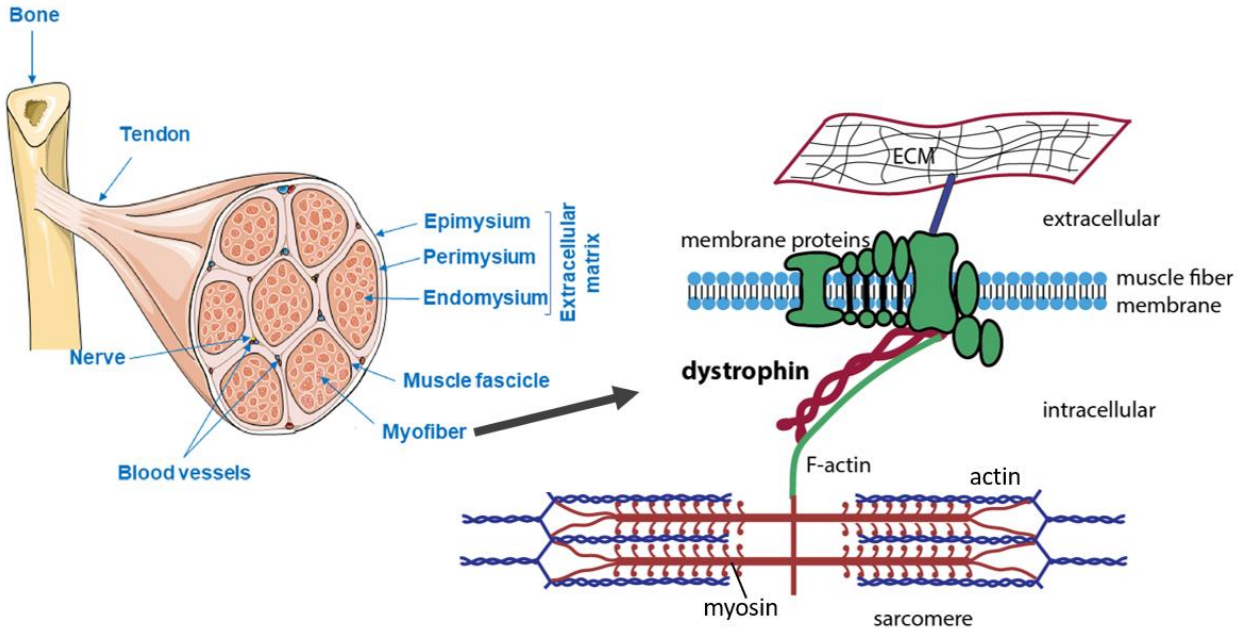

Figure 1.1 The hierarchical structure of skeletal muscle from the individual proteins comprising the sarcomere up to the whole muscle

Duchenne muscular dystrophy

Duchenne muscular dystrophy (DMD) is a recessive X-linked genetic disorder affecting 1 in 3500 boys and is caused by a mutation in the dystrophin gene that results in the incomplete translation of the dystrophin protein.[17,18] DMD is a progressive muscle wasting disease that dramatically impairs muscle function and tends to more significantly impact muscles of the lower limbs and the diaphragm. This impact on the diaphragm and the associated respiratory failure are one of the leading causes of mortality.[11,13] Despite extensive research, there remains no cure for DMD.

The absence of the dystrophin protein linking the intracellular sarcomere to the ECM weakens the structural integrity of the muscle and makes it more susceptible to contraction

induced damage.[1,2] This damage will occur during everyday actions such as walking, eating, and breathing. Constant cycles of damage and regeneration lead to a chronic state of inflammation in the muscle where ultimately, contractile muscle tissue is replaced by fibrotic tissue and fat.[3,4] These changes to the constituents of skeletal muscle have a negative impact on the force producing capabilities[5–7] as well as the passive properties[5,9,10] where fibrotic tissue is significantly weaker and stiffer than healthy tissue.

The *mdx* mouse is the most commonly used animal model to study DMD. While difficulties with replicating the disease phenotype seen in boys with DMD have occurred in limb muscles of mdx mice, the diaphragm has been shown to be a reliable model.[9]

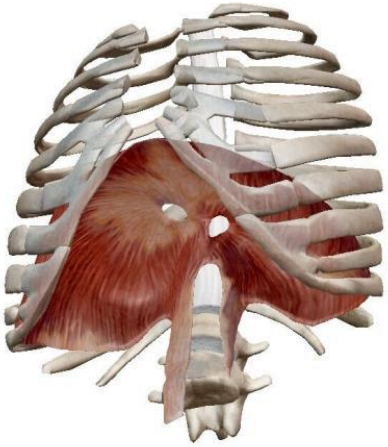

Figure 1.2*:* Illustration of the diaphragm muscle

Dystrophic diaphragm

One of the leading causes of mortality in DMD is cardiopulmonary failure believed to be caused by the weakening and dysfunction of the diaphragm as it is the primary driver of respiration.[12,13] The diaphragm is a large, dome shaped muscle that separates the thoracic and abdominal cavities. As the diaphragm contracts it displaces inferiorly, increasing the negative pressure in the pleural space thus causing the lungs to inflate. A magnetic resonance imaging study reconstructed diaphragm geometries from end-inspiration and end-expiration to measure diaphragm displacement during breathing and found a significant decrease in displacements in

boys with DMD compared to age-matched controls.[14] This study built upon our knowledge of respiratory impairment but was not able to delve into the changes in tissue mechanics that result in the measured dysfunction.

Skeletal muscle passive testing

Mechanical testing has long been the standard for evaluating the passive properties of various tissues. In skeletal muscle, studies have shown an increase in stiffness associated with muscular dystrophy[5,9,10,19] but this increase has not been found to be correlated with the increase in collagen characteristic of DMD.[10] Conversely, collagen digestion was found to be highly correlated with decreases in stiffness in healthy diaphragm tissue.[15] Despite the unique architecture and constraints of the diaphragm, the dystrophic diaphragm has only been investigated uniaxially. Evidence from healthy diaphragm has shown that both the along fiber and cross fiber directions should be considered and so biaxial tests are appropriate for the diaphragm.[20–22]

In order to understand the impact of fibrosis on passive mechanics, we need to be able to isolate the effects of collagen. Previous studies in cardiac mechanics have separated the total force response into a summation of each constituent through various tissue perturbations.[23,24] Through biaxial mechanical tests before and after enzymatic digestion of collagen, we can isolate the impact of collagen on both the along and across fiber passive properties.

Skeletal muscle active testing

Similar to passive testing, strips of muscle tissue are able to be tested to quantify the active mechanics of muscle. Previous experiments performing these *ex vivo* measurements have revealed both decreased force production and decreased shortening in the dystrophic diaphragm compared to healthy.[6,25] These muscle strip tests however are not able to maintain or replicate the complex physiologic conditions of the diaphragm such as the attachment of the central tendon, radial attachments to the ribs, or the presence of the transdiaphragmatic pressure. To truly measure the mechanics of the diaphragm, we must determine a way to

measure its function *in vivo*. Sonomicrometry has been successfully utilized to measure *in vivo* mechanics in cardiac tissue[26,27] for decades and has even been used to investigate the diaphragm in larger animals.[28–30] We built upon this previous research to adapt sonometric methods for use in the mouse to obtain both along fiber and across fiber measurements of diaphragm contraction.

Skeletal muscle modeling

Computational modeling is a powerful tool for simulating the complex behavior of tissues such as skeletal muscle. These models can reveal cause-effect relationships, ask "what-if" questions, simulate experiments that may be more logistically difficult, and develop new hypothesis. Early models simplified muscle architecture into Hill-type, lumped, one-dimensional models[31] and provided great insight into human movement but are limited in their ability to allow us to investigate deformations of complex geometries like that of the diaphragm or gain insight into changes due to diseases such as DMD.

More recent advances allow us to represent the muscle as a fiber-reinforced composite in three-dimensional finite element models.[16] This model assumes that the muscle is a transversely isotropic, hyperelastic, nearly incompressible material. This particular constitutive model uses an uncoupled form of the strain energy density function that separates the dilatational and deviatoric portions. It also uses physically based strain invariants which allows us to relate the material parameters of the model to our experimental measurements (Fig 1.3). Previously, this model of skeletal muscle has been used to investigate how strains in the biceps femoris may contribute to injury[32,33] and how muscles of the soft palate function during speech.[34] We will use this model to understand how the changes associated with DMD affect diaphragm function and then perform "what-if" simulations to investigate potential drug therapy targets.

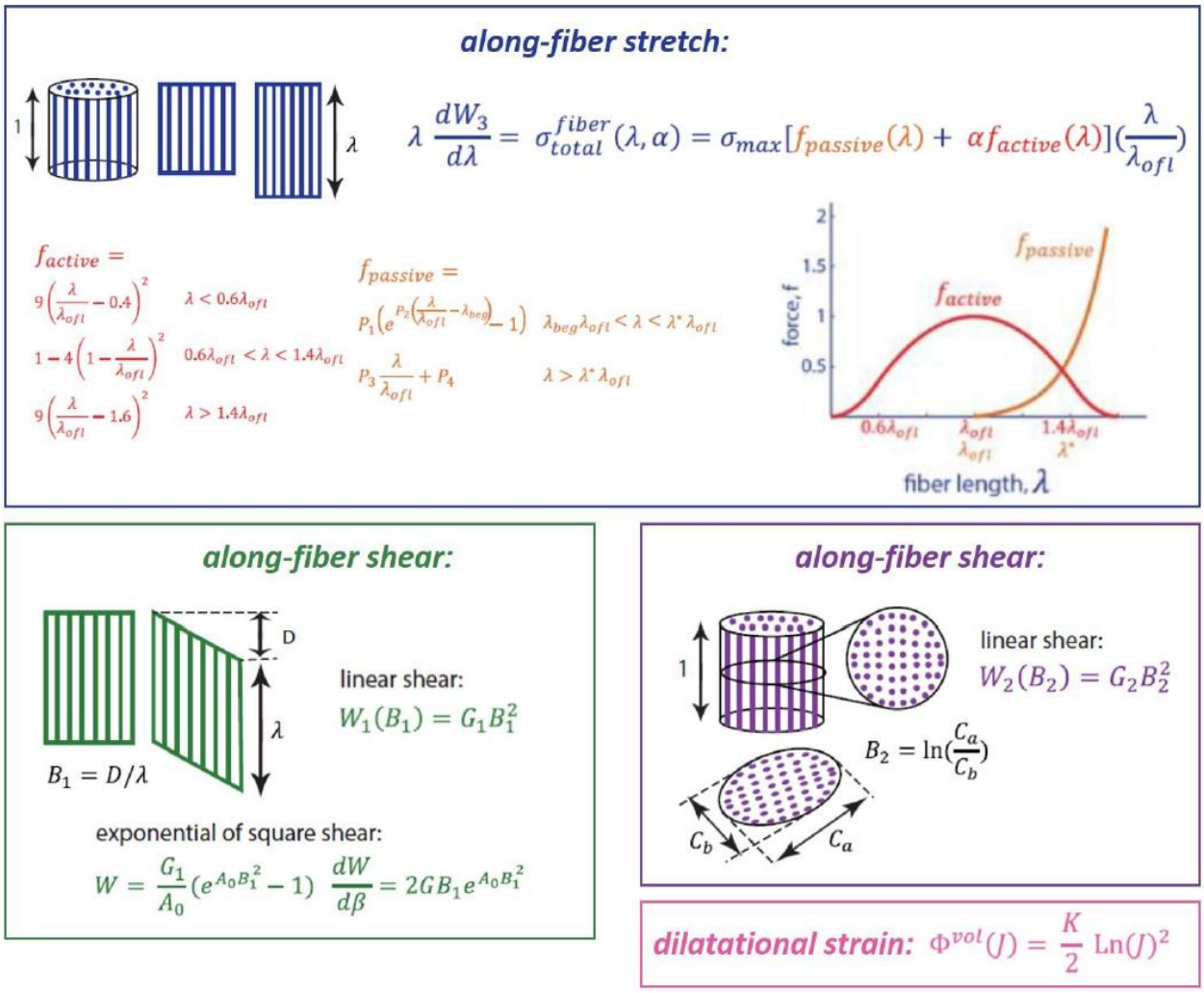

Figure 1.3: Skeletal muscle constitutive model

Chapter 2

Impact of collagen on the biaxial passive mechanical properties of diaphragm muscle tissue in wildtype and *mdx* mice

2.1 Abstract

Duchenne muscular dystrophy (DMD) is a progressive muscle wasting disease affecting 1 in 3500 boys. DMD is caused by the lack of the dystrophin protein, a structural protein linking the sarcomere to the extracellular matrix. Dystrophin's absence leads to an increased susceptibility to damage and thus everyday muscle use results in a chronic state of inflammation where healthy contractile tissue is replaced by fibrotic tissue and fat. This degeneration particularly affects the diaphragm muscle, the primary driver of respiration. How the altered constituents of the muscle tissue lead to its dysfunction are not well understood. Previous studies have demonstrated relationships between collagen and muscle stiffness while others have determined that collagen quantity cannot predict variations in muscle stiffness in dystrophic muscle. In this work, I performed biaxial mechanical tests on diaphragm samples from wildtype and dystrophic mice. Furthermore, I performed an enzymatic collagen digestion on each sample and repeated the biaxial protocol to investigate the isolated impact of collagen. In the along fiber direction, we found *mdx* samples to be significantly ($p=0.0131$, $p=0.0438$) stiffer than wildtype mice at both 3% and 8% strain. Similarly, in the across fiber direction we found *mdx* samples to be significantly ($p=0.0023$, $p=0.0002$) stiffer than wildtype mice at 3 and 8% strain. Following the digestion of collagen in *mdx* samples, they were no longer significantly stiffer than wildtype samples. Collagen amount was quantified through picrosirius red staining and a simple linear regression of collagen area fraction and the measured stiffnesses revealed significant positive correlations in the along fiber direction at 3% strain ($p=0.0380$) and in the across fiber direction at both 3% ($p=0.0149$) and 8% ($p=0.0323$) strain. However, R^2 values for these regressions were low indicating that more variability exists in the stiffness measurements than can be explained by collagen quantity alone. In this work, I demonstrated that a relationship exists between the collagen content of muscle and its stiffness and furthermore that this stiffness can

be returned to healthy levels through a reduction in collagen quantity providing a possible target for DMD therapies.

2.2 Introduction

Duchenne muscular dystrophy (DMD) is a fatal X-linked genetic disease affecting 1 in 3500 boys and is caused by an incomplete translation of the dystrophin protein.[18] The dystrophin protein is an integral structural protein responsible for linking the intracellular sarcomere to the extracellular matrix (ECM) and its absence leads to an increased susceptibility to muscle damage from everyday use.[17,35] The diaphragm muscle is particularly affected by DMD to the point that respiratory failure is one of the leading causes of mortality.[11–13] However, despite knowing the cause of the disease, development of better treatments for DMD is hampered by an incomplete understanding in the relationship between the structural changes associated with DMD and the muscle dysfunction.

The characteristic increased susceptibility to damage of DMD leads to a state of chronic inflammation where healthy muscle tissue is replaced by scar and fat.[4] This change in the constituents of muscle tissue will have an impact upon the mechanics but the exact role is not yet understood. Specifically looking at the unregulated fibrosis and excess collagen, there is evidence of both a relationship between collagen and muscle stiffness[15]; however, some studies have shown that collagen amount cannot predict variation in muscle stiffness across samples.[10,36]

Ex vivo passive testing of muscle tissue has long been the standard for evaluating tissue properties, like muscle stiffness, and has been applied to various muscles successfully. Furthermore, perturbations to the muscle to study individual constituents has been well established in cardiac mechanics[23,24] and also utilized in skeletal muscle mechanics.[15] Taken together, it is possible to isolate the effects of the unregulated fibrosis and study the impact of collagen on diaphragm muscle stiffness. Obtaining tissue samples, let alone those large enough

for passive testing, from boys with DMD is not feasible. Instead, the *mdx* mouse model of DMD is a well-studied and validated model of the disease whose diaphragm is able to replicate the phenotype seen in boys with DMD.[9,19]

The goal of this work is to investigate the impact of collagen on the passive biaxial properties of both healthy and dystrophic mouse diaphragm muscle tissue. This was accomplished through the passive mechanical testing of healthy and dystrophic mouse diaphragm muscle samples before and after an enzymatic collagen digestion.

2.3 Methods

Animals

In total, wildtype mice and mdx mice were used for ex vivo analysis. The Institutional Animal Care and Use Committee of the University of Virginia approved all animal procedures.

Sample dissection

Diaphragm isolation was performed in a manner to minimize tissue damage and preserve physiologically relevant lengths. Following euthanasia, the abdominal and thoracic cavities were opened, allowing pressure across the diaphragm to equilibrate. The diaphragm, ribs, and select vertebrae were then carefully excised together to preserve the attachment points and associated resting tension. Next the excised diaphragm was placed in a 100mm petri dish filled with chilled 2,3-butanedione monoxime (BDM), a relaxing solution that ensures that actin is not bound to myosin and thus not able to produce force places actin myosin cross-bridges in a pre-power-stroke state. Regions of interest from the lateral diaphragm were identified and four 30-gauge needles were used to pin the diaphragm to a piece of silicone to preserve its length and prevent tearing as five-by-five-millimeter samples were dissected. Contralateral sections of diaphragm were dissected in the same manner and thickness measurements were measured at nine evenly spaced locations using a laser displacement sensor (Keyence, Itasca, IL).

Ex vivo passive testing

Excised five-by-five-millimeter diaphragm muscle samples were mounted onto a CellScale Biotester which uses five rakes per side to create a uniform region of stretching in the center.[37] Samples were oriented so that the fibers were along one axis to minimize shear for the purpose of stress calculations. Samples were maintained in a chilled BDM bath throughout data collection to ensure only passive forces were measured.

Once mounted on the testing rig, samples were biaxially preloaded to a force of 10 mN in both directions. Sample size in this state was defined as the resting state and used as the basis for the strain-controlled loading protocol. Samples were cyclically stretched 10 times at strains of 5, 10, 15, and 20% at 1%/s with a 5-minute period of rest in-between strain levels. Images were taken at 1Hz for strain tracking.

Following data collection, the BDM bath was exchanged for a heated, 37C, bath of Liberase (Sigma), a blend of collagenase I and II and low concentration thermolysin, to enzymatically digest collagen from the muscle tissue samples. Samples were digested for ten minutes. Following this digestion, the chilled BDM bath was replaced and the same loading protocol was repeated. At the conclusion of passive force testing, samples were placed in formalin for histological analysis.

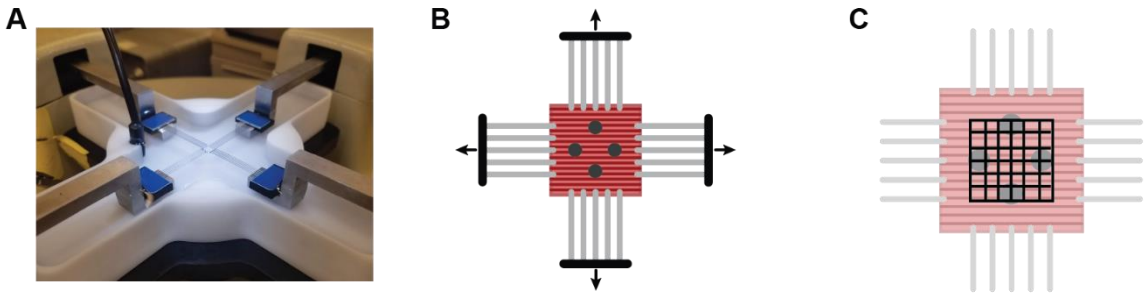

Figure 2.1: (A) Cellscale Biotester setup showing sample held by rakes attached to actuators in each axis. (B) schematic of diaphragm sample with dots for strain tracking and showing directions of stretch for equibiax testing. (C) representative grid for digital image correlation

Collagen quantification

Two samples per mouse, one from the passive testing and digestion protocol and the contralateral, were fixed in formalin, cleared, embedded in paraffin. Samples were sectioned in the transverse plane at 7-micron thickness and strained with picrosirius red. Collagen stained via picrosirius red is birefringent under circularly polarized light allowing for quantification of collagen.[38,39] Images were acquired at 10X magnification on an Olympus BX51 microscope. Bright field images were subtracted from polarized images to isolate collagen fibers from surrounding tissue and then the subtracted images were thresholded to differentiate collagen pixels from non-collagen. Collagen area fraction was then calculated from the number of collagen pixels to the total number of pixels in the sample. Sample fold changes in collagen area fraction were calculated from the contralateral sample and the digested sample from the passive testing protocol.

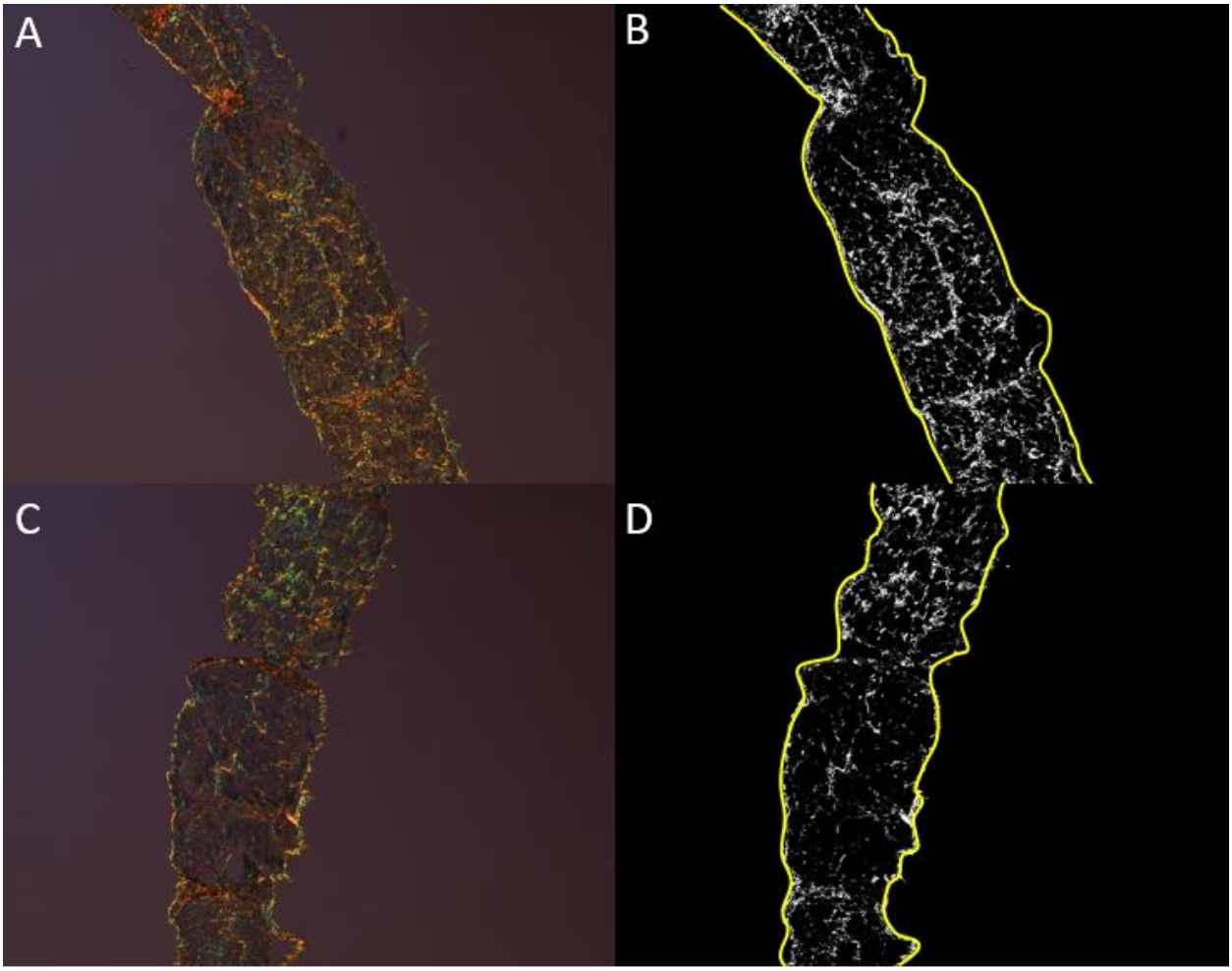

Figure 2.2: Circularly polarized light image of picrosirius stained section of diaphragm (A) before and (C) after enzymatic collagen digestion. (C, D) The same samples following thresholding and binarization with region of interest contained within yellow outline. Collagen pixels are shown as white and non-collagen as black.

Stress and strain calculations

The final cycle of the 10 stretches at each prescribed strain was used for analysis. This was chosen to ensure repeatable measurements in a quasi-static state to minimize viscoelastic contributions.

In-plane components of the deformation gradient, **F**, were calculated using strain tracking software developed by the Barocas Lab at the University of Minnesota.[40] The region of interest for strain tracking was defined by the innermost boundary of the rakes in each direction

to ensure a uniform region of interest and minimize edge effects from the points of attachment. Images of samples were examined for areas of the worst texture and minimum grid size necessary to capture pixel movement was calculated resulting in use of a five-by-five element grid.

A state of plane stress was assumed, so that all stress components involving the out-of-plane direction equal zero and that all out-of-plane deformations are also zero except those related to incompressibility meaning F is represented as:

$$[\boldsymbol{F}] = \begin{bmatrix} \lambda_1 & \kappa_1 & 0 \\ \kappa_2 & \lambda_2 & 0 \\ 0 & 0 & \lambda_3 \end{bmatrix} \qquad \text{Equation 2.1}$$

This allows us to compute the out of plane component of **F**, F33 as:

$$F_{33} = \lambda_3 = \frac{1}{(F_{11}F_{22} - F_{12}F_{21})} \qquad \text{Equation 2.1}$$

Cauchy stress, **t**, can be calculated using measured forces and cross-sectional areas:

$$\boldsymbol{f} = \boldsymbol{n} \cdot \boldsymbol{t}a \qquad \text{Equation 2.2}$$

where **f** is the force vector, **n** is the unit normal, and a is the current cross-sectional area. However, our measurements of cross-sectional area are taken in the undeformed configuration (A) so instead we used the first Piola-Kirchoff stress, **P**:

$$\boldsymbol{f} = \boldsymbol{N} \cdot \boldsymbol{P}A \qquad \text{Equation 2.3}$$

For our planar biaxial test, we oriented the fiber direction along a testing axis in order to assume that shear deformations are negligible. This was also verified via our strain tracking measurements. This means that the only nonzero stress components are

$$\mathrm{t}_{11} = \frac{\mathrm{f}_1}{a_1}, \qquad \mathrm{t}_{22} = \frac{\mathrm{f}_2}{a_2}$$

$$P_{11} = \frac{f_1}{A_1}, \; P_{22} = \frac{f_2}{A_2} \qquad \text{Equation 2.4}$$

where f1 and f2 are the forces along the testing axes, a_1 and a_2 are the current cross-sectional areas along those axes, and A_1 and A_2 the undeformed areas. 1st PK stress is related to Cauchy stress by

$$\boldsymbol{t} = \frac{1}{J}\boldsymbol{F} \cdot \boldsymbol{P} \qquad \text{Equation 2.5}$$

and the changing unit normal by

$$\boldsymbol{N}\, dA = \boldsymbol{n} \cdot \boldsymbol{F}\frac{da}{J} \qquad \text{Equation 2.6}$$

Knowing that our only forces are along the testing axes, we can substitute equation into equation and solve for P:

$$\mathrm{P}_{11} = \lambda_2\lambda_3\mathrm{t}_{11}$$

$$\mathrm{P}_{12} = -\kappa_1\lambda_3\mathrm{t}_{22} = \left(\frac{-\kappa_1}{\lambda_1}\right)\mathrm{P}_{22}$$

$$\mathrm{P}_{21} = -\kappa_2\lambda_3\mathrm{t}_{11} = \left(\frac{-\kappa_2}{\lambda_2}\right)\mathrm{P}_{11}$$

$$P_{22} = \lambda_1\lambda_3 t_{22} \qquad \text{Equation 2.7}$$

This still assumes that all deformed cross-sectional areas are known but they usually are not so looking at equation in the along fiber axis, we get

$$N_1A_1 = \frac{1}{J}n_1a_1 \cdot F = \frac{a_1}{J}[1 \quad 0 \quad 0] \cdot \begin{bmatrix} \lambda_1 & \kappa_1 & 0 \\ \kappa_2 & \lambda_2 & 0 \\ 0 & 0 & \lambda_3 \end{bmatrix} = \frac{a_1}{J}[\lambda_1 \quad \kappa_1 \quad 0] \qquad \text{Equation 2.8}$$

so then it follows that

$$N_1 = \frac{1}{\sqrt{\lambda_1^2+\kappa_1^2}}[\lambda_1 \quad \kappa_1 \quad 0] \qquad \text{Equation 2.9}$$

and

$$A_1 = \frac{a_1}{J}\sqrt{\lambda_1^2 + \kappa_1^2} \qquad \text{Equation 2.10}$$

With a known relationship between the undeformed and current cross-sectional area and knowing that J=1 for incompressible materials, we are able to solve for Cauchy stress as[26]:

$$t_{11} = \frac{f_1}{A_1}\sqrt{\lambda_1^2 + \kappa_1^2}$$

$$t_{22} = \frac{f_2}{A_2}\sqrt{\lambda_2^2 + \kappa_2^2} \qquad \text{Equation 2.11}$$

where f1, t11 and f2, t22 are the measured forces and Cauchy stress in the along fiber and across fiber directions, respectively, and λ and κ are components of the deformation gradient **F** calculated using the strain tracking software. Along-fiber versus cross-fiber stresses are all shown in Figure A2 in Appendix A.

The Lagrangian strain was calculated as

$$\boldsymbol{E} = \frac{1}{2}(\boldsymbol{C} - \boldsymbol{I}) = \frac{1}{2}(\boldsymbol{F}^T\boldsymbol{F} - \boldsymbol{I}) \qquad \text{Equation 2.12}$$

Where **F** is the deformation gradient and **I** is the identity matrix. Along-fiber versus cross-fiber strains for all samples are shown in Figure A1 in Appendix A.

Stiffness Calculation

Peak Cauchy stress and Lagrangian strain from the final cycle at each prescribed strain rate were used to create a curve representing the quasi-static response for each sample (Fig A3). Each curve was then fit to a second order polynomial. A second order polynomial was chosen to avoid issues with overfitting associated with higher order polynomials and the large variability in parameter space associated with exponentials. Once fit, the instantaneous slope at 3% and 8% strain was calculated to represent the stiffness at a lower and higher strain.

Statistics

Stiffness and collagen area fraction measurements were compared using a 3-way ANOVA with disease, age, and digestion as the independent variables and Tukey's post-hoc test if significance was found with the ANOVA. A simple linear regression was performed on stiffness versus collagen area fraction measurements.

2.4 Results

In the along fiber direction, we found a significant difference ($p=0.0131$, $p=0.0438$) between wildtype and dystrophic mice at both 3% and 8% strain (Fig2.3A, C). There was also a significant difference ($p=0.0112$) between wildtype 12-month-old mice (0.925 ± 0.216 MPa) and dystrophic 12-month-old mice (4.589 ± 3.589 MPa) at 3% strain (Fig2.3A). It is also of note that following digestion, there was no longer a significant difference between the native wildtype muscle and the digested dystrophic muscle. At both 3% and 8% strain, there was a significant difference ($p=0.0037$, $p=0.0227$) in stiffness between native and digested samples in 12-month-old dystrophic mice.

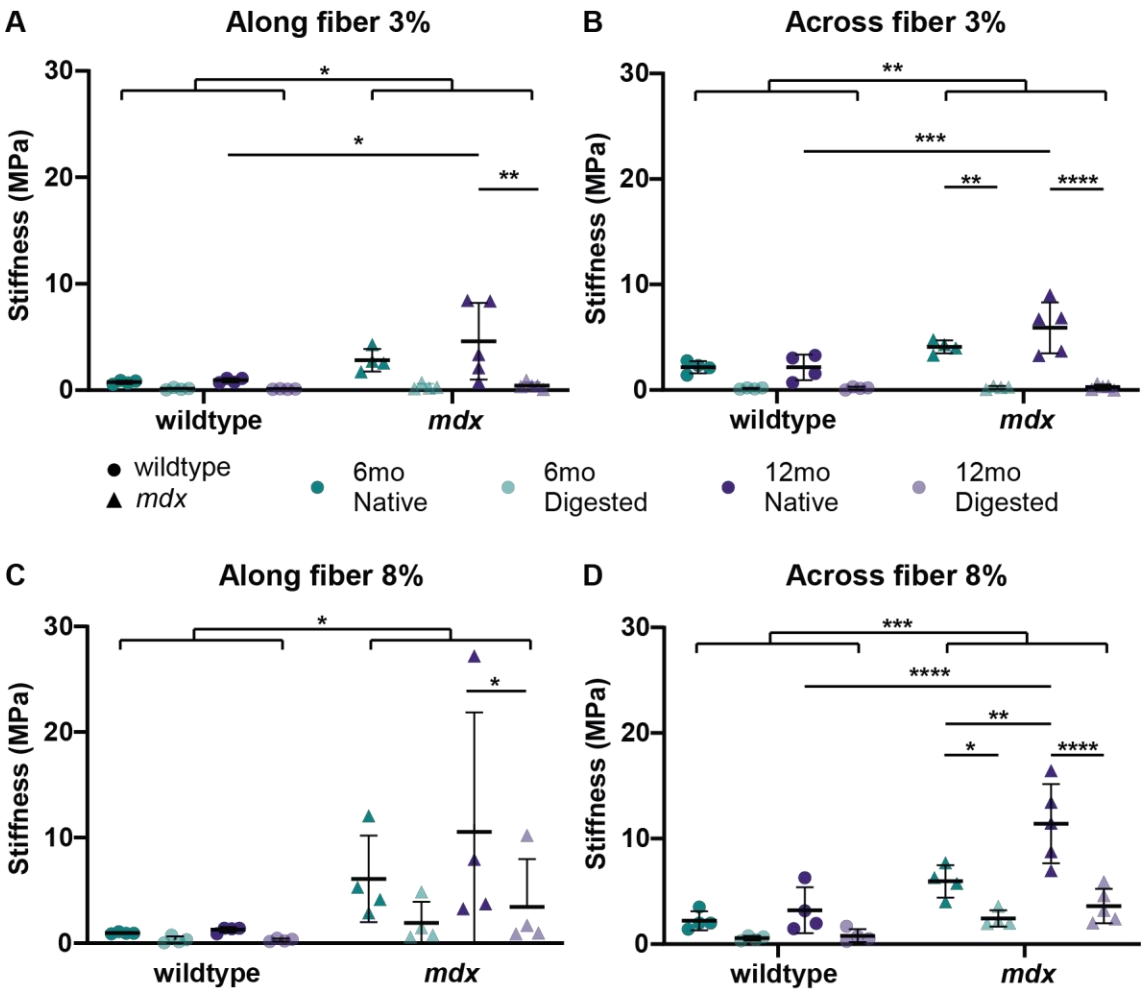

Figure 2.3: Stiffness measurements in the along fiber direction at (A) 3% strain and (C) 8% strain and in the across fiber direction at (B) 3% strain and (D) 8% strain

In the across fiber direction, we found a significant difference (p=0.0023, p=0.0002) between wildtype and dystrophic mice at 3 and 8% strain (Fig2.3B, D). Similar to the along fiber direction, there is a significant difference (p=0.0002, p<0.0001) between the 12-month-old wildtype (2.151 ± 1.223 MPa, 3.212 ± 2.168 MPa) and 12-month-old dystrophic (5.904 ± 2.406 MPa, 11.411 ± 3.751 MPa) mice at both 3 and 8% strain (Fig2.3B, D). Again, following digestion this difference is no longer significant (p=0.3591, p>0.9999) at both 3 and 8% strain. There is also a significant difference (p=0.0026) between 6-month-old (5.953 ± 1.539 MPa) and 12-month-old (11.411 ± 3.751 MPa) dystrophic mice at 8% strain (Fig2.3D). Finally, there is a

significant difference in stiffness due to digestion for both 6 and 12-month-old dystrophic mice at 3 and 8% strain (Fig2.3B, D).

Measurements of collagen area fraction show a significant difference ($p<0.0001$) between 6-month-old wildtype (5.51 ± 1.11 %) and dystrophic (14.17 ± 1.49 %) mice (Fig2.4). This relationship remained significant ($p<0.0001$) following digestion despite a significant ($p=0.0092$) decrease in collagen in the dystrophic mice. Considering the dystrophic mice, there is a significant difference ($p=0.0031$) between 6-month-old and 12-month-old mice both before (6mo: 14.17 ± 1.49 %, 12mo: 8.68 ± 2.16 %) and after (6mo: 10.63 ± 2.16, 12mo: 4.94 ± 2.65 %) digestion.

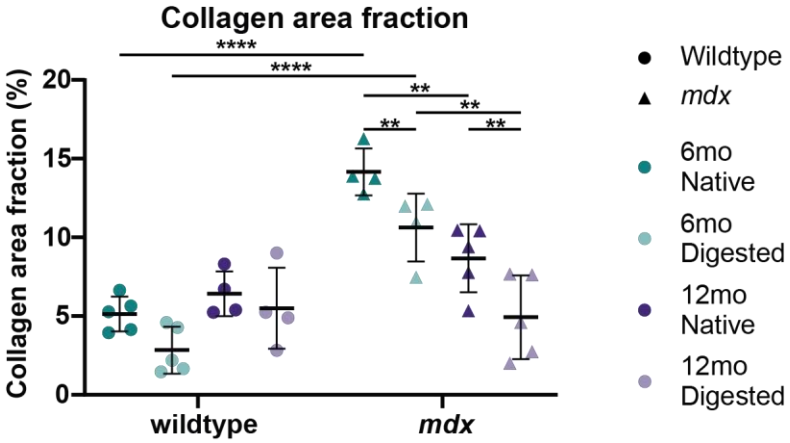

Figure 2.4: Measurements of collagen area fraction as quantified by picrosirius red straining

A simple linear regression of collagen area fraction and stiffness revealed significant positive correlations in the along fiber direction at 3% strain ($p=0.0380$) and in the across fiber direction at 3% ($p=0.0149$) and 8% strain ($p=0.0323$) (Fig 2.5A, C, D).

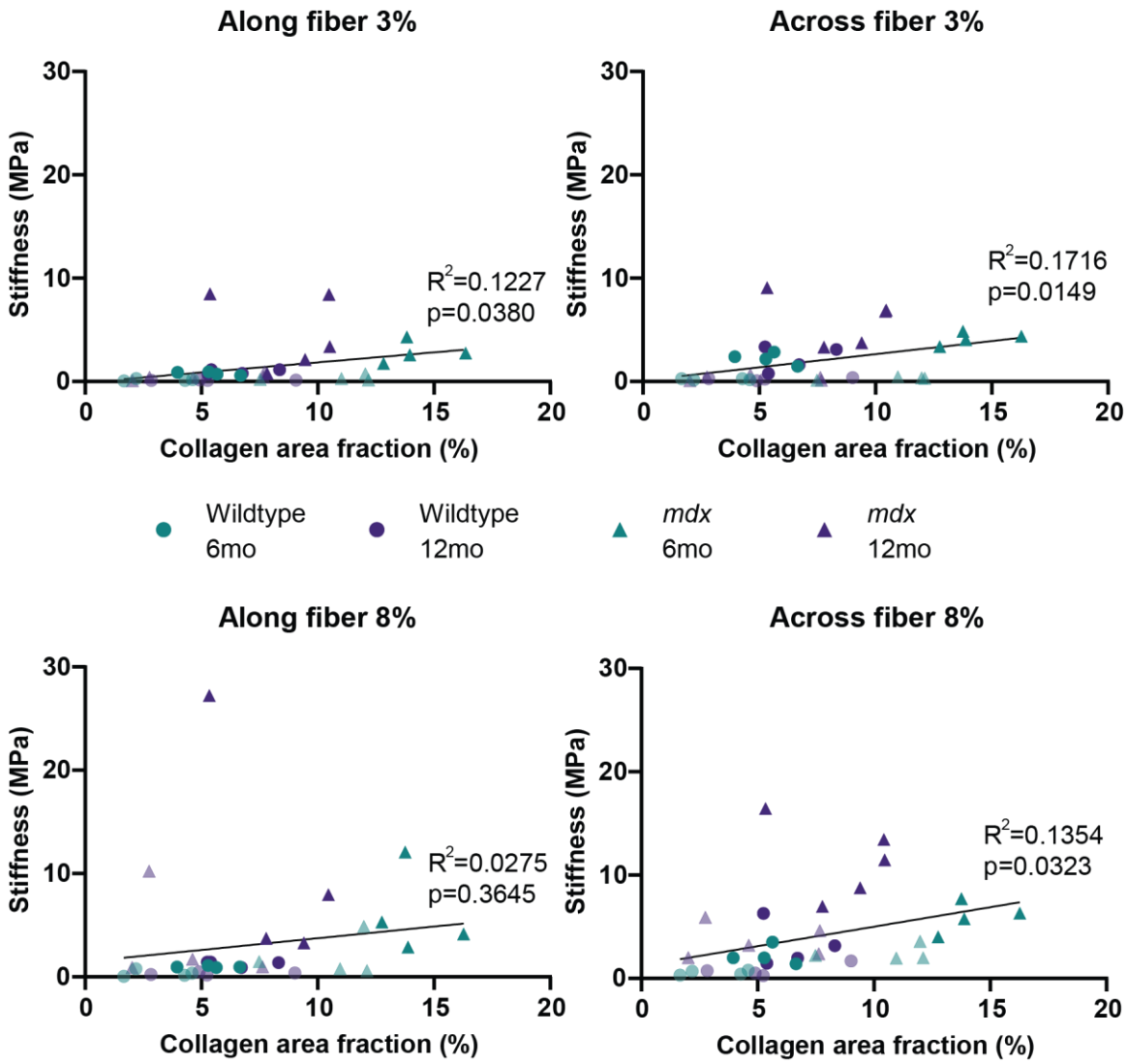

Figure 2.5: Collagen area fraction compared to along fiber stiffness at (A) 3% strain and (B) 8% strain and across fiber stiffness at (C) 3% strain and (D) 8% strain

2.5 Discussion

The overall goal of this work was to investigate the impact of collagen on the passive mechanics of healthy and dystrophic diaphragm in both the along and across fiber direction. This was accomplished through planar biaxial mechanical testing of diaphragm tissue samples from wildtype and *mdx* mice before and after enzymatic collagen digestion. Digestion of collagen was verified through image analysis of picrosirius red stained sections and revealed significant decreases in the percent collagen before and after digestion in the dystrophic samples as well

as between 6-month-old wildtype and mdx mice. Stiffness calculations of measured stress strain data revealed significant differences between wildtype and mdx mice as expected. Futhermore, digestion of collagen resulted in a significant decrease for all *mdx* samples except the along fiber 6-month-old mice. Finally, significant correlations were found between collagen area fraction and along fiber stiffness at 3% strain as well as between collagen area fraction and across fiber stiffness at 3 and 8% strain.

Increased stiffness in the along fiber direction of dystrophic muscle has been well established by previous studies[5,9,10,19] however all of these studies were conducted in the along fiber direction only. Differential behavior in the along and across fiber directions have been noted in the diaphragm[21,22] however the dystrophic diaphragm has not yet been studied biaxially to our knowledge. Interestingly, the across fiber direction appears to be more significantly impacted by the disease state and increased fibrosis at both low and high strain percentages. The effects of collagen digestion also appear to be more significant in the across fiber direction. This could potentially be due to the orientation of the collagen as the newly laid down collagen will be in response to current mechanical loads which are shown to dictate collagen direction.[41]

Collagen area fraction measurements showed increased collagen quantity in dystrophic muscle compared to healthy muscle as expected.[10] We are also given confidence in our methods as our digestion protocol caused a significant decrease in the collagen content of our dystrophic mice. Initial experiments involved a more thorough digestion but these samples were unable to withstand a second round of the passive testing protocol to assess changes in muscle stiffness. Despite this significant decrease in collagen quantity following digestion, the digested dystrophic muscle still had significantly more collagen than the native healthy muscle. This is of particular interest when combined with the findings from the passive testing, that the stiffness between the two groups was no longer significant. Taken together, it is possible that future therapies do not need to return collagen quantities to healthy levels, only to reduce them far enough to return muscle stiffness to baseline.

Finally, significant correlations between collagen area fraction and muscle stiffness were noted at low strains in the along fiber direction and at high and low strains in the across fiber direction. This absence of correlation at higher strains in the along fiber direction agrees with previous studies.[10,36] Low R2 values show that even with a significant trend between the two variables, collagen quantity alone is not able to fully explain the variability in stiffness measurements across samples. This could be due to variability in our measurements or there may be another factor, such as collagen orientation, to consider and warrants further investigation.

This study was not without its limitations, the largest being the limited sample size of each group. Low samples sizes will decrease the statistical power of our analysis which is not ideal considering the high variability of our data, especially within the *mdx* mice groups. Previous work analyzing individual constituent contributions digested the rest of the constituents leaving only the one of interest.[24,42] Instead, we chose to isolate the effects of collagen by only digesting the collagen and investigating how the response changed. Without repeated studies utilizing each method, it is impossible to determine if one method is more effective. However, the alternative approach would have decreased difficulties associated with losing samples due to overdigestion where not enough collagen remained to give the sample the integrity needed for passive testing. We chose to employ collagen digestion to limit total testing time as muscle properties will begin to change with time following excision from the animal.

In conclusion, this work demonstrates that collagen is significantly correlated with the measured stiffness of the diaphragm muscle in both the along fiber and across fiber directions. Additionally, we found that a significant decrease in collagen quantity through enzymatic digestion of dystrophic muscle was able to restore stiffness values to those of healthy muscle.

Chapter 3

Sonomicrometry of *mdx* mouse reveals that diaphragm dysfunction involves diminished along-fiber and cross-fiber strains during inspiration

3.1 Abstract

Duchenne muscular dystrophy (DMD) results in a progressive degeneration of skeletal muscle that particularly affects the diaphragm, the main driver of respiration. Clinical measurements of lung volume reveal decreased respiratory function in boys with DMD and magnetic resonance imaging (MRI) studies show a corresponding decrease in diaphragm displacement. In order to develop targeted therapies to restore respiratory function, we need to understand the regional *in vivo* mechanics of the diaphragm which MRI is unable to capture. In this study, we adapted a technique commonly used in cardiac research known as sonomicrometry in order to asses diaphragm function in vivo. We then used this method to investigate changes in diaphragm function with disease progression in the *mdx* mouse using sonomicrometry. Strain measurements revealed shortening strains in the along-fiber direction and lengthening strains in the cross-fiber direction in both wildtype and mdx mice at all ages. Both along-fiber and cross-fiber strains were significantly lower in diseased mice at 6 months old (along: wt=-0.092±0.042 *mdx*=-0.028±0.012; cross: wt=0.119±0.047 *mdx*=0.036±0.011, $p<0.001$) but not at 12 months old (wt=-0.069±0.038 *mdx*=-0.072±0.058; cross: wt=0.039±0.011 *mdx*=0.036±0.016, $p>0.99$). Strain rates in diseased mice were also significantly lower than those in the healthy mice (wt=0.87±0.39 *mdx*=0.41±0.099, $p<0.01$). Passive biaxial testing was used to approximate *in vivo* residual stress which revealed a significant decrease in cross-fiber stretch in diseased mice compared to healthy. Our results indicate clear regional changes in diaphragm mechanics associated with disease progression that must be considered in the development of treatment plans and therapeutics for patients with DMD.

3.2 Introduction

Duchenne muscular dystrophy (DMD) is a fatal X-linked genetic disease caused by a mutation in the dystrophin gene that results in its incomplete translation. The dystrophin protein is a structural protein whose absence leads to increased susceptibility to damage from everyday muscle use.[17,35] This damage affects every skeletal muscle, however those in the lower limbs and the diaphragm, appear to be more significantly affected. As this damage to the diaphragm worsens with disease progression, the boys begin to require assistance with respiration and their reliance on assistive devices increases with age. Ultimately, cardiopulmonary failure associated with respiratory dysfunction is the leading cause of mortality for boys with DMD. [11–13]

The primary muscle that actuates respiration is the diaphragm muscle. The diaphragm is a large, dome shaped muscle that separates the thoracic and abdominal cavities. As the diaphragm contracts, an increase in negative pressure within the pleural space causes the lungs to fill with air. Spirometry measurements in clinic reveal a significant decrease in pulmonary function in boys with DMD. A magnetic resonance imaging (MRI) study revealed a significant reduction in the displacement of the diaphragm in boys with DMD compared to age-matched controls, and displacements continued to decrease with age in boys with DMD. [14] This reduction in displacement may decrease the amount of negative pressure created within the plural space and thus explain the decreased pulmonary function observed in clinic.

While MRI is able to capture the decreased movement of the diaphragm that is associated with worsened pulmonary function, it is unable to discern the regional mechanical changes that lead to this reduction in movement. While measuring changes in regional motion within the diaphragm in boys with DMD is impractical, the *mdx* mouse diaphragm is a more accessible model that is also able to recapitulate the pathology of the diaphragm muscle.[9] Previous *ex vivo* studies have shown decreased force production[5] as well as increased passive stiffness[10] however due to the diaphragms unique pennation, attachments, and central tendon,[43]

it is difficult for *ex vivo* studies to fully replicate *in vivo* mechanics. Passive regional mechanics of the whole rat diaphragm have been measured via pressure loading in an *ex vivo* setup and revealed anisotropic behavior[22] confirming the need to consider regional behavior. Currently, studies measuring the *in vivo* mechanics are limited: ultrasound has been used in a method similar to the MRI study to observe diaphragm displacements and decreases were noted in the *mdx* mouse compared to healthy controls.[44] Regional tissue behavior that is able to discern the behavior of the muscle fibers would be more informative towards the development of improved therapies as DMD is a multifaceted disease without a current cure. Identifying which parts of the pathology i.e., decreased force production, increased fibrosis, fatty infiltration, etc., to target will help improve the care of boys with DMD.

Sonomicrometry has been reliably utilized to measure *in vivo* regional muscle tissue strains in cardiac[26,27] as well as skeletal[45,46] muscle, including the diaphragm[28–30] of larger animals. The use of individual ultrasound crystals allows for high resolution measurements in smaller areas, like the costal region of the diaphragm. To our knowledge, sonomicrometry has not yet been used to study the *in vivo* mouse diaphragm or the effects of muscular dystrophy on the regional mechanics of the diaphragm. Therefore, the goals of this study were to i) develop a method for using sonomicrometry to measure along-fiber and cross-fiber strains of the mouse diaphragm and ii) investigate changes in diaphragm function with disease progression in the *mdx* mouse using sonomicrometry.

3.3 Methods

In Vivo Strain Measurements

We measured diaphragmatic strains *in vivo* in 22 mice using sonomicrometry. All experiments were approved by the University of Virginia Animal Care and Use Committee. Male wildtype C57BL/6J and C57BL/10ScSn-Dmdmdx/J (referred to as *mdx*) mice at age 6 and 12 months (Jackson Laboratory, Bar Harbor, ME) were anesthetized and maintained on oxygen and 1-2%

isoflurane. The abdominal cavity was opened via a midline incision, exposing the inferior side of the diaphragm muscle. A cautery pen was then used to fully expose the left hemidiaphragm. The left side was chosen due to less obstruction from abdominal organs. The point at which the descending aorta passes through the central tendon of the diaphragm was located and a pair of piezoelectric crystals (Sonometrics, London, ON, Canada) were glued to the muscle tissue lateral to this anatomical marker about 3-4 mm apart in the along-fiber direction of the muscle. A second pair of crystals was glued perpendicular to the first pair, in the cross-fiber direction. The test area was covered in ultrasound gel and crystal displacements were recorded during 7-10 continuous breaths. Data were acquired at 1000 Hz using the commercial software SonoLab (Sonometrics). Mouse respiration rate was monitored throughout testing to ensure it did not fall too low due to anesthesia and we also later verified that there were no significant differences in respiration rate between any of the groups. Following data collection, the piezoelectric crystals were gently removed from the diaphragm, using tissue dye to mark their location. Mice were euthanized using isoflurane inhalation and a bilateral thoracotomy. The diaphragm was removed and placed in cold 2,3-butanedione monoxime (BDM, Sigma-Aldrich, St.Louis, MO) to prevent muscle contracture.

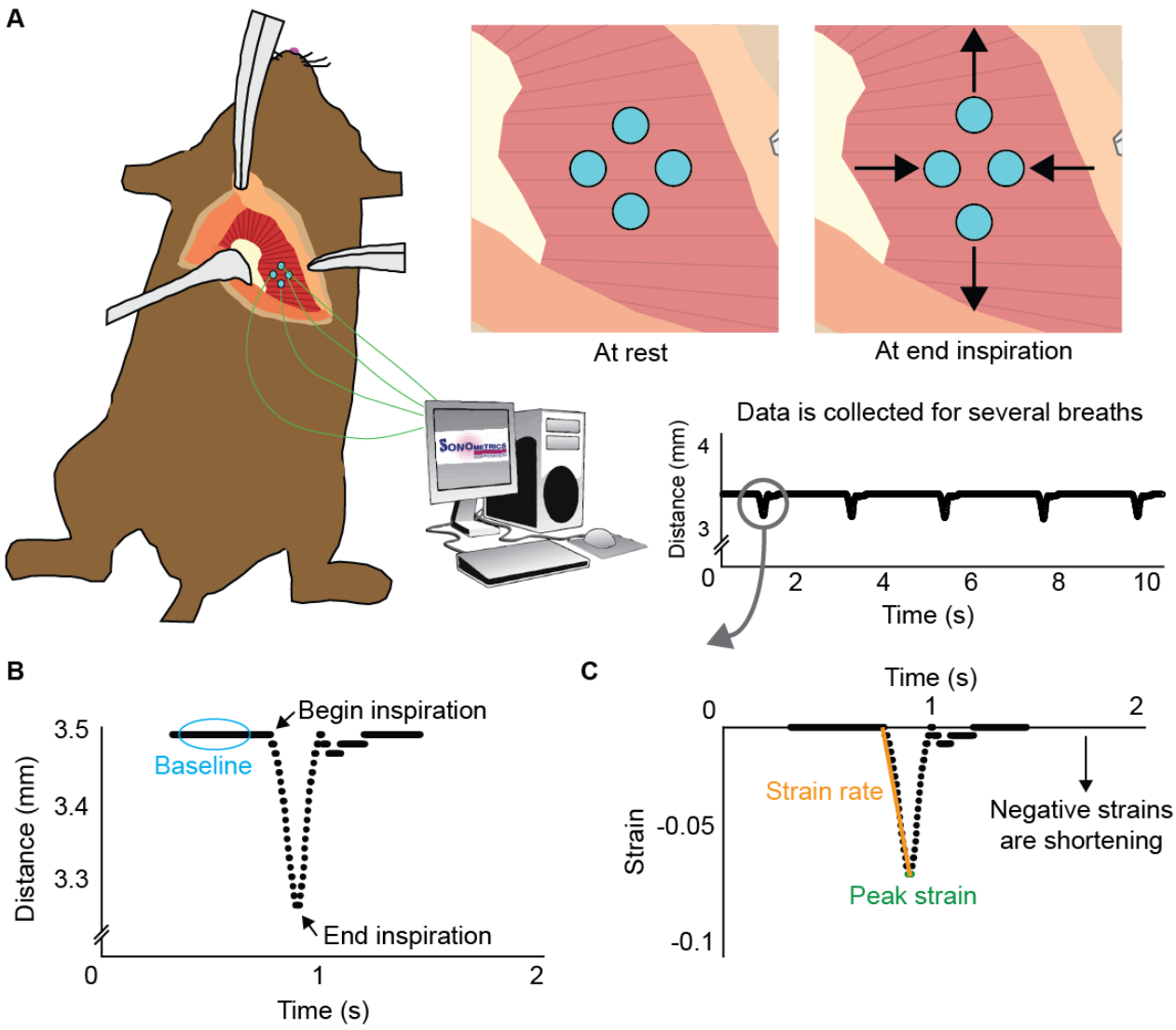

Figure 3.1: (A) Experimental setup depicting four ultrasound crystals glued to the inferior side of the left hemidiaphragm. One pair of crystals is oriented in the along-fiber direction and the other in the cross-fiber direction. Sonometrics software is used to collect distance measurements as the mouse breathes. (B) Zoom in on one breath to show the raw distance data for the along-fiber direction. The baseline distance between crystals is used to calculate strains. (C) Zoom-in of along-fiber strain. Shortening strains are represented as negative and lengthening as positive. Peak strain is the strain at end inspiration and strain rate was calculated as the slope of the line from begin to end inspiration.

In vivo strains were calculated using the distance recorded between crystals between breaths as the baseline value. Shortening strains are reported as negative values and lengthening as positive. Strain rate was calculated as the slope of the line from begin-inspiration to peak strain. Strains and strain rates were then compared between ages and between healthy and dystrophic mice using an ANOVA and Tukey's test for post-hoc analysis. Along-fiber or

cross-fiber strain data were excluded if a reliable signal could not be measured. Final group sizes were n=6 for 6-month-old wildtype along-fiber and 12-month-old wildtype along-fiber. For all other groups, n=5.

Residual Stretch Calculation

Following the completion of *in vivo* testing, diaphragm samples were explanted and stretched biaxially to determine the length at which passive resistance is measurable. The *in vivo* data and *ex vivo* data were then related through the distances between the crystals in the sonomicrometry experiments and the tissue dye markers in the passive mechanical testing. By creating this parallel, we are able to determine the amount of residual stress within the diaphragm. The distance between the crystals *in vivo* was divided by the distance between the tissue markers where passive resistance was measured and called the resting stretch. Resting stretches were compared between ages and between healthy and dystrophic mice using an ANOVA and Tukey's test for post-hoc analysis. Due to the fragility of the mouse diaphragm, some samples tore during loading for passive stretching; final n for each group were 4 for 6-month-old wildtype, 5 for all other groups.

Collagen quantification

Two samples per mouse, one from the sonomicrometry and passive testing protocol and the contralateral, were fixed in formalin, cleared, embedded in paraffin. Samples were sectioned in the transverse plane at 7-micron thickness and strained with picrosirius red. Collagen stained via picrosirius red is birefringent under circularly polarized light allowing for quantification of collagen.[38,39] Images were acquired at 10X magnification on an Olympus BX51 microscope. Bright field images were subtracted from polarized images to isolate collagen fibers from surrounding tissue and then the subtracted images were thresholded to differentiate collagen pixels from non-collagen. Collagen area fraction was then calculated based off of number of collagen pixels to the total number of pixels in the sample. Sample fold changes in collagen

area fraction were calculated from the contralateral sample and the digested sample from the passive testing protocol.

Stiffness measurements

This method and data are discussed at length in Chapter 1. Briefly, diaphragm samples were cyclically stretched to prescribed strains of 5, 10, 15, and 20% in the along fiber and across fiber directions equibiaxially. Strain tracking was used to obtain the deformation gradient in order to calculate lagrangian strain and Cauchy stress. Instantaneous stiffness measurements were calculated at 3 and 8 percent strains.

3.4 Results

Sonomicrometry measurements of *in vivo* mouse diaphragm confirmed that fibers shorten along their length during inspiration (Fig 3.2A). There was a significant ($p=0.0392$) decrease in the magnitude of along-fiber strains between the wildtype (-0.0916 ± 0.0424) and mdx (-0.0278 ± 0.012) mice at 6 months; however, there were no significant differences in along-fiber strain between wildtype and mdx at 12 months. While fibers shorten along their length, the diaphragm muscle tissue lengthens in the cross-fiber direction during inspiration (Fig 3.2B). There was a significant ($p<0.0001$) decrease in cross-fiber strains between the wildtype (0.1187 ± 0.0472) and mdx (0.0358 ± 0.0111) mice at 6 months old. A significant ($p=0.0001$) decrease was also seen with aging in the wildtype mice from 6 months (0.1187 ± 0.0472) to 12 months old (0.0392 ± 0.0108).

Strain rates measured in wildtype mice were significantly higher than those in *mdx* mice (wt = 0.87 ± 0.39 *mdx* = 0.41 ± 0.099, $p=0.0026$) (Fig 3.3A). A significant correlation ($p<0.0001$) was found between strain rate and along-fiber strain (Fig 3.3B).

There was a significant ($p=0.0242$) decrease in resting along-fiber stretch with aging in wildtype mice between 6-month-old (1.3329 ± 0.3091) and 12-month-old (0.8376 ± 0.0804) mice. A significant ($p=0.0079$) difference was found with regards to disease state between the

wildtype (1.3113 ± 0.3517) and mdx (0.9795 ± 0.2296) mice in the cross-fiber direction (Fig 3.4B).

Collagen area fraction measurements were significantly different ($p<0.0001$) between wildtype and dystrophic mice at 6 months of age but not at 12 months ($p=0.2026$). These results are shown in Figure 2.4 and discussed more in depth in Chapter 2. A simple linear regression of the measured collagen area fractions and along and across fiber strains was performed revealing a significant correlation in the along fiber ($p=0.0133$) and across fiber ($p=0.0133$) direction (Fig3.5A, B). However, strain rates in both the along and across fiber directions were not significantly correlated with collagen area fraction (Fig3.5C, D).

Finally, we compared measured *in vivo* strains to the *ex vivo* stiffnesses discussed in Chapter 1. No significant correlations were found between the sonomicrometry strains and the passive testing stiffnesses in the along fiber or cross fiber directions at high or low strains (Fig3.6).

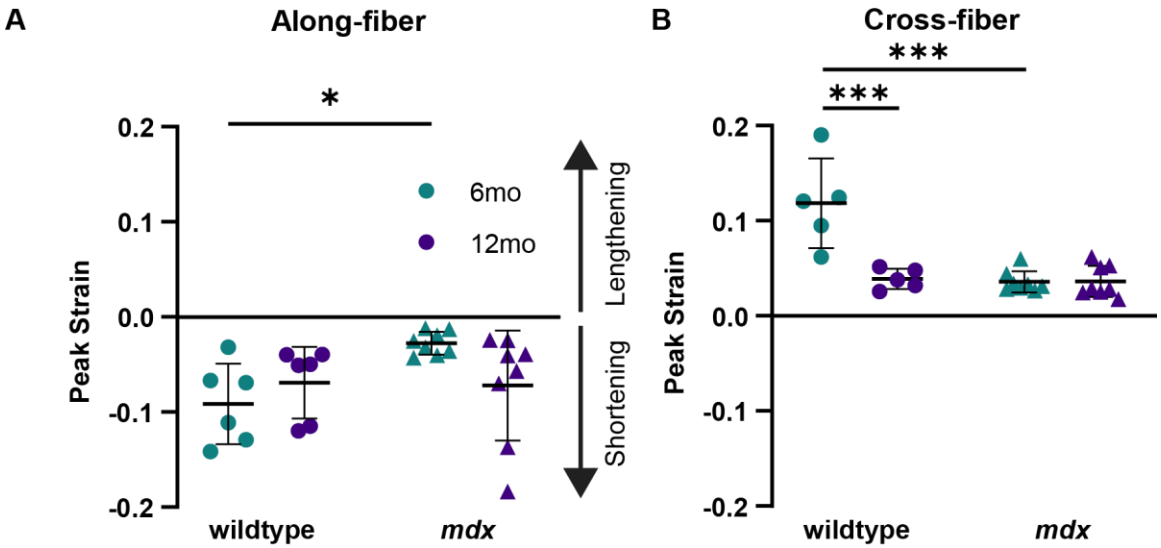

Figure 3.2: A) Along-fiber peak strains during tidal inspiration. Negative strains represent shortening. (B) Cross-fiber peak strains during inspiration, positive strains represent lengthening. Significance shown between groups with bars, where * is p<0.05, ** is p<0.01, and *** is p<0.001.

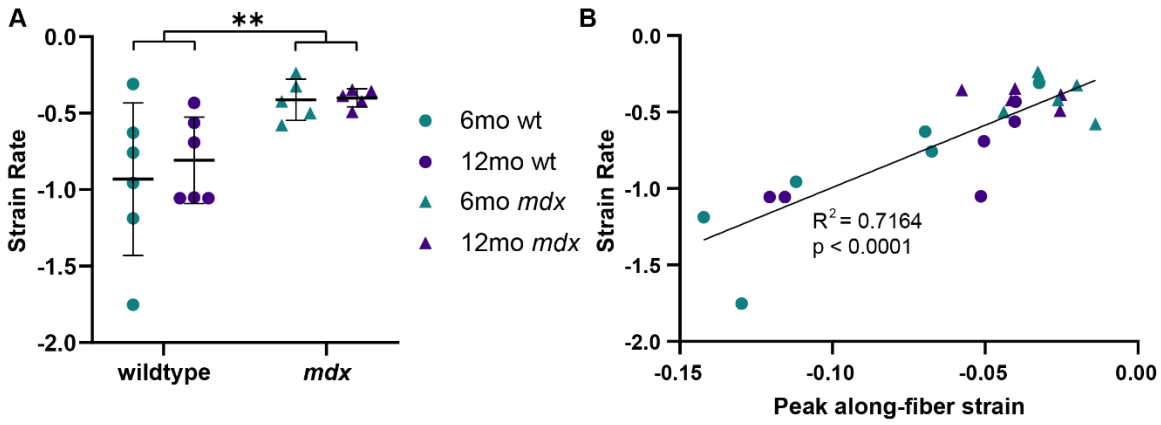

Figure 3.3: (A) In vivo along-fiber strain rates during inspiration. (B) Linear regression between along-fiber strain and strain rate for mdx and wildtype mice. Negative strains and strain rates represent shortening. ** is p<0.01

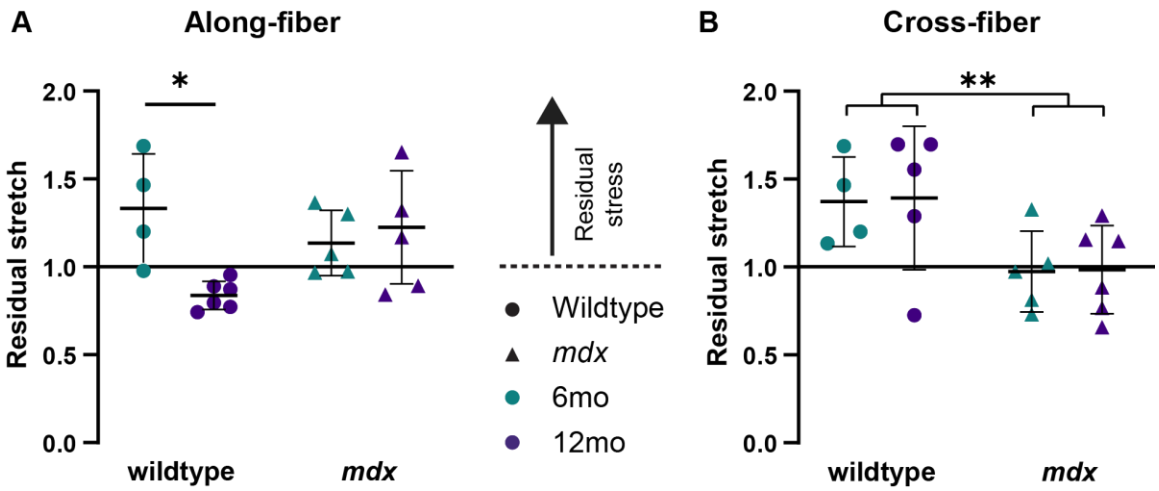

Figure 3.4: (A) Residual stretch in the along-fiber direction of the diaphragm at its between-respiration length. Stretches above 1.0 signify a residual stress present. (B) Corresponding cross-fiber residual stretch. Significance shown between groups with bars, where * is $p<0.05$ and ** is $p<0.01$.

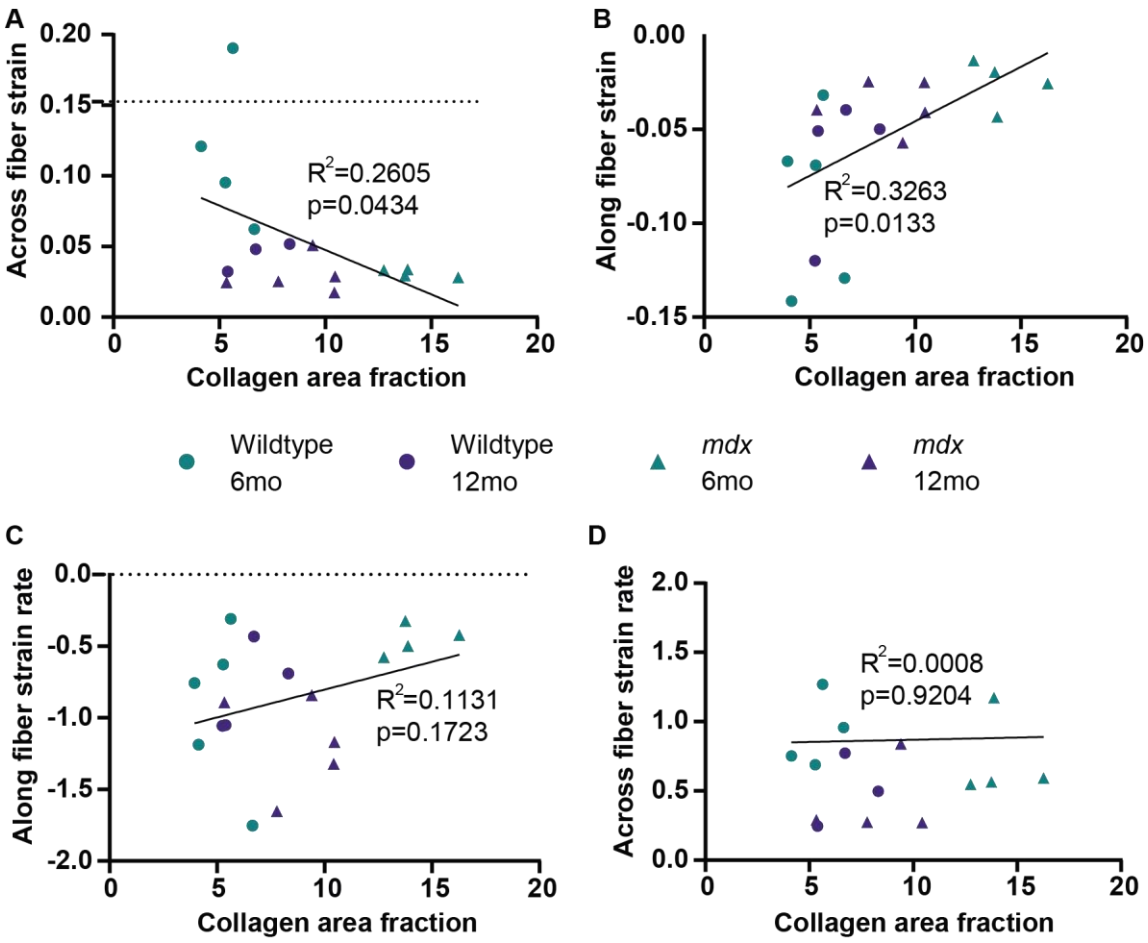

Figure 3.5: (A) Linear regressions between collagen area fraction as measured by polarized light imaging of picrosirius red stained sections and (A) along fiber strain, (B) across fiber strain, (C) along fiber strain rate, and (D) across fiber strain rate. Negative strains represent shortening.

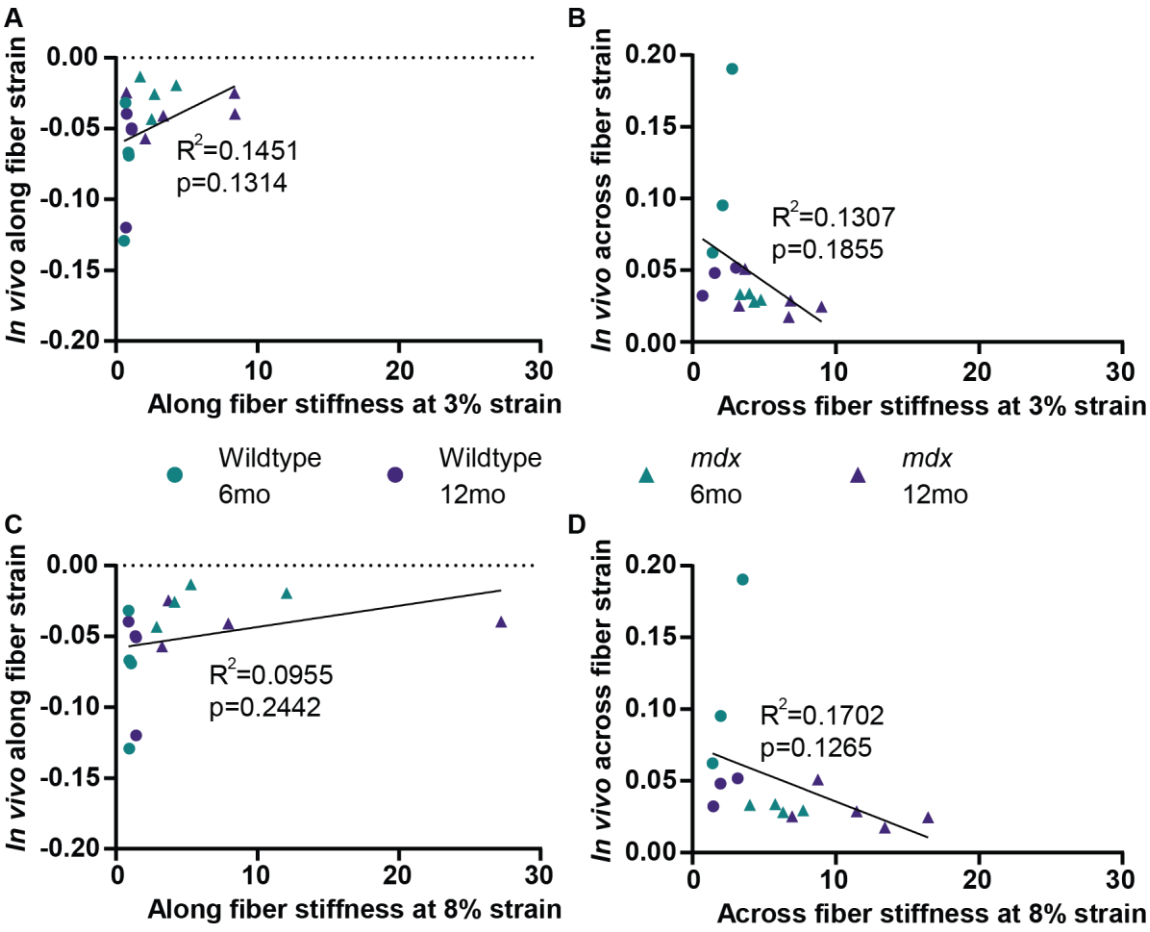

Figure 3.6: Linear regressions between measured in vivo along fiber strains and calculated ex vivo along fiber stiffnesses at (A) 3% and (C) 8% strains. Regressions between measured in vivo across fiber strains and calculated ex vivo across fiber stiffnesses at (B) 3% and (D) 8% strains. Negative strains represent shortening.

3.5 Discussion

The overall goal of this work was to measure if, and to what extent, regional strains are impaired in the *mdx* diaphragm. Our first goal of this study was to adapt sonometric methods to measure regional along-fiber and cross-fiber strains of the *in vivo* mouse diaphragm. We accomplished this by gluing piezoelectric crystals to the inferior side of the diaphragm of anesthetized mice and measuring regional tissue displacements during spontaneous breathing. Our measurements of diaphragm contraction during inspiration revealed shortening strains in the along-fiber direction and lengthening strains in the cross-fiber direction. We then used this

method to accomplish our second goal, investigating regional mechanical changes in the dystrophic diaphragm of the *mdx* mouse. Our study revealed that the dystrophic diaphragm has lower strains in both the along-fiber and cross-fiber direction as well as lowered along-fiber strain rates. Residual cross-fiber stretch was also lowered in the *mdx* mice compared to wildtype. Comparing measured strains to collagen area fraction, known to be elevated in dystrophic muscle, a significant correlation was found in the along fiber direction but not the across fiber direction.

Our adaptation of sonomicrometry for measurement of *in vivo* along-fiber and cross-fiber diaphragm strains provides a unique perspective of the muscle mechanics and its changes due to muscular dystrophy that typical methods have previously been unable to capture. Similar to other skeletal muscles, as the diaphragm contracts, along-fiber strains shorten while cross-fiber strains lengthen. This is of particular interest when considering the fan shape of the diaphragm, its movement during contraction, and how this movement is altered in states of dysfunction. Duchenne muscular dystrophy is characterized by its excessive fibrosis, which is known to alter the mechanics of tissues. However, prior to this work, how fibrosis affects the specific along and cross-fiber behavior of the dystrophic diaphragm is not yet fully understood. Measurements of strips of diaphragm have found decreased peak force and peak shortening in *mdx* diaphragm[6,25] however these are usually conducted at optimum fiber length as measured by twitch force. A previous study from our group measured differing *in vivo* sarcomere lengths between wildtype and *mdx* mice[47] suggesting that measuring at optimum fiber length may not accurately represent *in vivo* function. *Ex vivo* strip tests do not capture the cross-fiber behavior of the diaphragm as it has been removed from its highly unique physiologic attachment consisting of a fan-shaped architecture that will contribute to lateral force transmission as well as attachment to a dynamic central tendon and ribs. Cross-fiber behavior is of particular interest in fibrotic diseases such as DMD where we expect excess collagen to be deposited in nonuniformly. Our measurements of regional mechanics capture both the *in vivo* along-fiber and

cross-fiber mechanics and suggest that muscular dystrophy lowers both along and cross-fiber strains as well as along-fiber strain rates. This result agrees with clinical data of boys with DMD having lowered functional lung volumes as measured by spirometry.

In addition to lowered strains, diseased diaphragms also exhibited lower residual stretch. The mechanism behind the lower observed residual stretch in the diseased diaphragms could be one of two possibilities. If the mechanical properties of the tissue have not changed, a lower residual stretch would be a result of a lowered residual stress. However, the fibrotic nature of muscular dystrophy may cause such drastic changes to the structural and material properties of the muscle tissue[9,10] that the lower residual stretch may be associated with either the same or even higher residual stress. The impact of fibrosis and collagen deposition on the dystrophic diaphragm remain debated in the literature but it is generally accepted that dystrophic muscle is stiffer than healthy muscle.[10,15] To gain additional insight into the residual stress present in the diaphragm, future work would be necessary to investigate the passive mechanics of the diaphragm at the *in vivo* residual stretches measured.

DMD is characterized by a chronic state of inflammation and associated unregulated fibrosis. This results in significantly elevated quantities of collagen within the muscle. Comparing the collagen area fraction of each sample to its measured strains, we found a significant correlation in the along and across fiber directions. Interestingly however, along and across fiber strain rates were not significantly correlated despite the previously discussed highly significant relationship between along fiber strain and strain rate.

Our results also showed that aging is associated with lowered strain measurements in wildtype but not *mdx* mice. Aged wildtype mice exhibited lowered cross-fiber strains and along-fiber residual stretch. Changes in the cross-fiber but not the along-fiber strain suggest that the changes due to aging may not be related to the contractile abilities of the muscle but rather to the passive mechanics of the tissue. Interestingly, no significant changes were noted with aging in the *mdx* mice suggesting that at 6 months of age, the diaphragm is already significantly

impacted in this model of DMD and disease progression does not cause further changes in diaphragm mechanics. This is in contrast to previous ultrasound experiments which measured a lowered diaphragm excursion at 18 months compared to 8 months.[44] It is possible that further disease progression occurs after 12 months of age. Alternatively, it is also possible that by measuring the regional mechanics only, we are isolating the muscle from other physiological changes associated with DMD such as changes to the properties of the central tendon and changes to the shape and movement of the ribcage. Indeed, MRI studies have noted a change in thoracic cavity size and movement during respiration[48], both of which will affect diaphragm excursion measurements.

There are several potential limitations of this study that should be discussed. The *mdx* mouse, despite some limitations, is a widely used and accepted model for studying the functional changes due to DMD. The limb muscles of the mouse do not fully capitulate the pathology of DMD and have seen issues with translation from benchtop to clinic, however, the diaphragm most closely resembles the pathological changes seen in DMD and is an acceptable muscle to study.[9] Use of this animal model also allows us to employ novel experimental methods to probe the functional changes that occur as a result of muscular dystrophy in new ways to provide a better understanding of the disease. A potential source of error in our experiment can be attributed to the use of anesthesia during the sonomicrometry experiments. Isoflurane, a respiratory depressant, has been shown to reduce both respiratory rate and tidal volume. To minimize this potential affect, the depth of anesthesia was carefully monitored and adjusted for each animal throughout the procedure to ensure a steady state of spontaneous breathing. Furthermore, we calculated the breathing rate for each mouse and found no significant differences between our groups suggesting that all differences found between groups were due to disease or age and not an effect of the anesthesia. Finally, we glued the crystals to the muscle tissue rather than sewing them as has been done in previous studies with larger animals.[26–30,45,46] An analysis by Newman et al found no significant differences in tidal

shortening between glued and sewn crystals in dog diaphragm[28] so we expect gluing the crystals should also not affect the measurements in mice. Additionally, glue is the recommended method of attachment for the smaller crystals by Sonometrics. By gluing the crystals to the surface of the diaphragm we also made the assumption that the signal would travel through the ultrasound gel only. We believe this is a valid assumption as the mouse diaphragm is more planar than the human, and the region of interest for our measurements does not undergo drastic changes in curvature during inspiration.

This study has found several interesting changes in the in vivo behavior of the dystrophic diaphragm, and provided unique measures that compliment previous *in vivo* ultrasound studies of the mouse diaphragm. The next challenge will be to understand how all of these changes interrelate, which is quite difficult to ascertain through experiments alone. Finite element models have been used to study various complex muscles in ways that we typically are not able to with standard benchtop experiments.[16,34] A finite-element model of the diaphragm model would allow for probing of the differences between the sonomicrometry and ultrasound data by allowing the manipulation of the ribcage boundary conditions and central tendon properties in accordance with other studies.

To conclude, our results demonstrate sonomicrometry as a viable method of measuring *in vivo* diaphragm function of the mouse in both the along-fiber and cross-fiber directions providing a unique perspective on muscle function and how that may change in a diseased state such as DMD. The ability to measure regional muscle function in its physiologic state provides a significant advantage over traditional *ex vivo* methods and other *in vivo* methods in the context of understanding muscle pathophysiology. We employed our method to study DMD in the *mdx* mouse model and found significantly lowered along-fiber and cross-fiber strains as well as along-fiber strain rates in diseased mice compared to wildtype mice. Through establishment of this baseline difference, our method can now be used to investigate potential therapeutics and

isolate their effect on the diaphragm muscle separate from other pathological changes known to occur due to DMD.

Chapter 4

A 3D model of the diaphragm muscle to elucidate the roles of active and passive muscle mechanics on diaphragm dysfunction in DMD

4.1 Abstract

Duchenne muscular dystrophy (DMD) is a genetic disorder that results in the progressive replacement of healthy contractile muscle tissue with fibrotic tissue and fat. This degeneration particularly affects the diaphragm muscle ultimately resulting in cardiopulmonary failure, the leading cause of mortality for boys with DMD. Clinical assessments via spirometry and magnetic resonance imaging studies have confirmed the impact of DMD on respiration and the diaphragm, respectively. However, the degree to which the altered active, reduction in contractile tissue, and passive, increase in fibrotic tissue, mechanics result in this dysfunction remains unclear. To elucidate the role of the active and passive mechanics on diaphragm function, we built and tuned a finite element model of the mouse diaphragm and performed "what-if" simulations to predict how restoration of the active and passive mechanics independently would improve diaphragm function. Model simulations predicted a 75% recovery with restoration of active mechanics and a 35% with passive. Our results highlight the need to consider not only the active mechanics of dystrophic muscle but also the passive in our goal of improving the lives of boys with DMD.

4.2 Introduction

Duchenne muscular dystrophy (DMD) is a fatal X-linked genetic disease characterized by the lack of the dystrophin protein. The dystrophin protein is a structural protein whose absence leads to increased susceptibility to damage from everyday muscle use.[17,35] This damage affects every skeletal muscle, however some muscles degenerate more quickly than others. Degeneration of the diaphragm muscle leads to boys with DMD requiring assistance with respiration that typically increases with age usually ending with reliance on a ventilator. Ultimately, cardiopulmonary failure associated with respiratory dysfunction is the leading cause of mortality for boys with DMD. [11–13]

The diaphragm is a large, fan-like muscle that separates the thoracic and abdominal cavities and its contraction along with other smaller muscles drives respiration through an increase in negative pressure in the thoracic cavity. Diaphragm dysfunction is typically assessed clinically through spirometry but a magnetic resonance imaging (MRI) study revealed a significant decrease in the superior-inferior displacement of the diaphragm in boys with DMD that increased with age and disease progression.[14] A similar measurement of diaphragm displacement has more recently been performed on wildtype and *mdx*, a DMD model, mice using ultrasound and revealed similar trends between mdx mice and boys with DMD.[44]

Despite advancements in knowledge of the dysfunction of the diaphragm and novel ways to measure and track changes in function, the cause of the dysfunction remains unclear. The high susceptibility to damage associated with DMD leads to chronic inflammation, fibrosis, and impaired regeneration ultimately resulting in drastically altered active and passive mechanics of the muscle.[49] Numerous studies have been conducted showing decreased force production associated with DMD.[5–8] There is also well documented changes to the passive properties of dystrophic muscle showing that it is significantly stiffer than healthy muscle.[5,9,10] Furthermore, chapter 3 of this dissertation revealed that both along- and cross-muscle fiber properties are impaired in dystrophic muscle. However, the degree to which these altered active and biaxial passive mechanics contribute to the overall dysfunction of the diaphragm is not well understood.

The overall goal of this chapter is to elucidate the individual impacts of the altered active and passive mechanics associated with DMD on overall diaphragm function. To achieve this goal, we built a finite element model of the mouse diaphragm that was then informed by experimental data from wildtype and mdx mice. We then used the model to perform simulations

to examine the changes in diaphragm function associated with the changes to the mechanical properties due to DMD.

4.3 Methods

Model geometry

Diaphragm muscle images of a C57BL/6J mouse taken on a 7T MR scanner with 50 μm spatial resolution from The Visible Mouse project[50] were segmented using a Matlab (Mathworks Inc., Natick, MA) software package that was developed in the Multiscale Muscle Mechanopysiology lab at the University of Virginia.[51] In each image, the diaphragm muscle was identified and its boundary outlined. A three-dimensional (3D) diaphragm muscle geometry was then created by fitting splines to the z-stacked outlines.

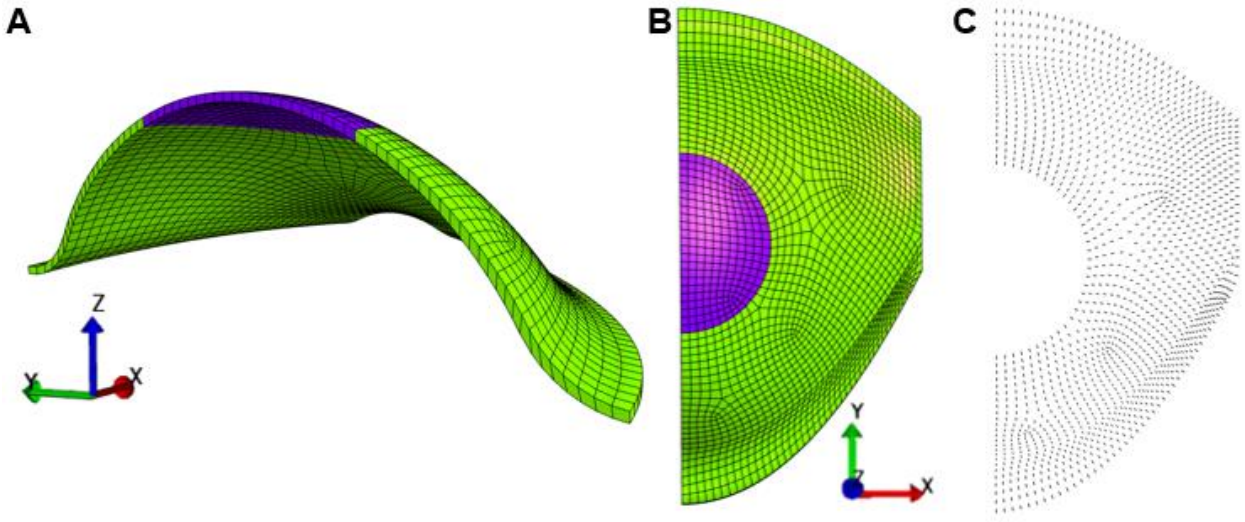

Figure 4.1: (A, B) Model geometry showing central tendon in purple and muscle in green. (C) Muscle fiber directions for each muscle element of the model

The segmented geometry was imported to Autodesk Inventor (Autodesk Inc., San Rafael, CA) where splines from cross sections at the midline and edge of the diaphragm were taken. A surface was then lofted between the two following the geometry from the MR

segmentation to create the final 3D geometry. The central tendon was identified in the MR images and a simplified circular geometry was imprinted on the Inventor model.

Model fiber direction

The 3D geometry was meshed into 3D hexahedral elements (Coreform Cubit, Orem, UT). The model contains 1799 elements, 1559 comprising the muscle and 240 the central tendon.

Fiber direction was determined for each element using a previously described method utilizing Laplacian simulations.[52] For the Laplacian simulation, fibers were directed from the musculotendon junction (inlet surface) to the insertion at the ribs (outlet surface).

Across fiber direction was then determined by calculating the cross product of the fiber vector and the normal of the face of the element.

Constitutive model

Muscle was modeled as a mixture of two transversely isotropic, hyperelastic, quasi-incompressible materials[16], one in the along fiber direction and a second in the across fiber direction, and the central tendon as a neo-Hookean material. The transversely isotropic, hyperelastic, quasi-incompressible muscle material has the strain energy density function:

$$\Phi(\boldsymbol{C}, \boldsymbol{a}_0) = W_1 + W_2 + W_3 + \Phi^{vol} \quad \text{Equation 4.1}$$

where $\mathbf{a}_0$ is the local fiber direction and **C** is the right Cauchy-Green deformation tensor. $W_1 = G_1(B_1)^2$ and $W_2 = G_2(B_2)^2$ where G_1 and G_2 represent the along fiber and across fiber shear modulus, respectively. G_1 was set to zero and G_2 was 0.01 for wildtype mice and 0.1 for dystrophic mice. The term W3 defines the relationship between the Cauchy stress in the fibers ($\sigma_{\text{total}}^{\text{fiber}}$), the fiber stretch (λ), and the activation level (α):

$$\lambda \frac{\delta W_3^{muscle}}{\delta \lambda} = \sigma_{total}^{fiber}(\lambda, \alpha)$$ Equation 4.2

where Cauchy stress in the fibers is:

$$\sigma_{total}^{fiber}(\lambda, \alpha) = \sigma_{max} f_{total}^{fiber}(\lambda, \alpha) \frac{\lambda}{\lambda_{ofl}}$$ Equation 4.3

$\sigma_{\max}$ is the max isometric stress and defined as 225 kPa for wildtype mice and 90 kPa for dystrophic mice.[44] The total fiber force, $f_{\text{total}}^{\text{fiber}}(\lambda, \alpha)$, can be represented as a sum of the active and passive force:

$$f_{total}^{fiber}(\lambda, \alpha) = f_{passive}^{fiber}(\lambda) + \alpha f_{active}^{fiber}(\lambda)$$
Equation 4.4

This normalized passive fiber force is defined by the following piece-wise function:

$$f_{\text{passive}}^{\text{fiber}}(\lambda) = 0 \qquad \lambda \leq \lambda_{\text{ofl}}$$

$$f_{\text{passive}}^{\text{fiber}}(\lambda) = P_1 \left(e^{P_2 \left(\lambda / \lambda_{\text{ofl}} - 1 \right)} - 1 \right) \qquad \lambda_{\text{ofl}} < \lambda < \lambda^*$$

$$f_{passive}^{fiber}(\lambda) = P_3 \frac{\lambda}{\lambda_{ofl}} + P_4 \qquad \lambda \geq \lambda^*$$ Equation 4.5

where λ^* represents the fiber stretch at which the passive curve becomes linear and P_3 and P_4 are defined such that the curve is C_0 and C_1 continues at $\lambda = \lambda^*$. λ^* is defined as 1.1 for all mouse models due to theoretical fittings showing a shortened toe region. The parameters characterizing the passive force response, P_1-P_4, were determined by fitting passive mechanical testing data from Chapter 2 to a finite element model of the biaxial test.

Passive fiber force parameter optimization

A simple slab model was created to simulate the planar equibiaxial mechanical test from Chapter 2. The model was 3 mm x 3mm x 0.2 mm and composed of 16 hexahedral elements. A

displacement of 0.45 mm was applied to the positive x and y faces. The negative x and y faces as well as the negative z face were all fixed in their respective directions. The built in FEBio parameter optimization module[53] was then used to solve inverse finite element problems such that the optimized values of P_1 and P_2 lead to stress values predicted by the model that matched the measurements made in Chapter 3. P_3 and P_4 are automatically calculated by the software based off of the curve continuity previously discussed.

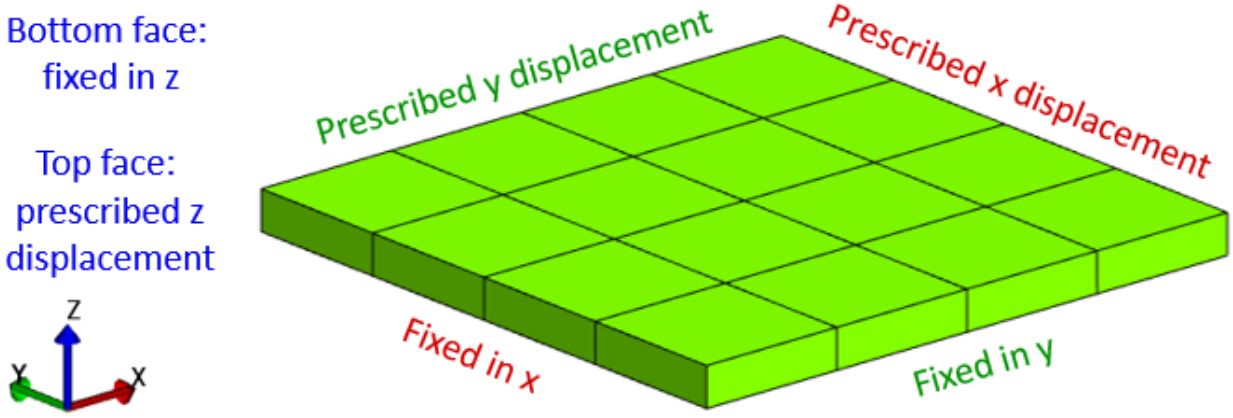

Figure 4.2: Slab model geometry

Model boundary conditions

Due to an assumption of symmetry and only modeling one half of the diaphragm, the midline of the diaphragm is fixed in the x-direction. Additionally, the area where the diaphragm would insert on the ribs is fixed in the z-direction, preventing superior/inferior displacements. Finally, the elements where the diaphragm would insert towards the spine are fixed in x, y, and z as we've assumed this area would be rigid in the system.

To simulate the negative transdiaphragmatic pressure that is necessary for respiration a 1 kPa surface pressure[54] was applied in the superior direction to the inferior face of the diaphragm and central tendon.

Calculating strains and diaphragm amplitude

In order to compare the model predictions with the sonomicrometry data described in Chapter 3, four nodes in the model of the diaphragm were identified in a region that would be similar to the area sonomicrometry crystals were placed for strain measurements in Chapter 3. The first node was identified and then a second by taking the fiber direction from the element of that node and following it to a second a few millimeters away. This pair of nodes represents the along fiber direction. The across fiber direction was determined by identifying an additional pair of nodes along a vector orthogonal to the fiber direction. Position data from the four nodes was output throughout the simulation and Euclidian distance between the nodes was calculated to obtain along fiber and across fiber strains from the model.

In order to compare the model predictions with diaphragm amplitude measurements found in the literature[44], diaphragm amplitude is typically defined as the superior-inferior displacement of the diaphragm muscle tendon unit. Z displacement, which measures superior-inferior displacement in the model, of the central tendon was calculated throughout simulations.

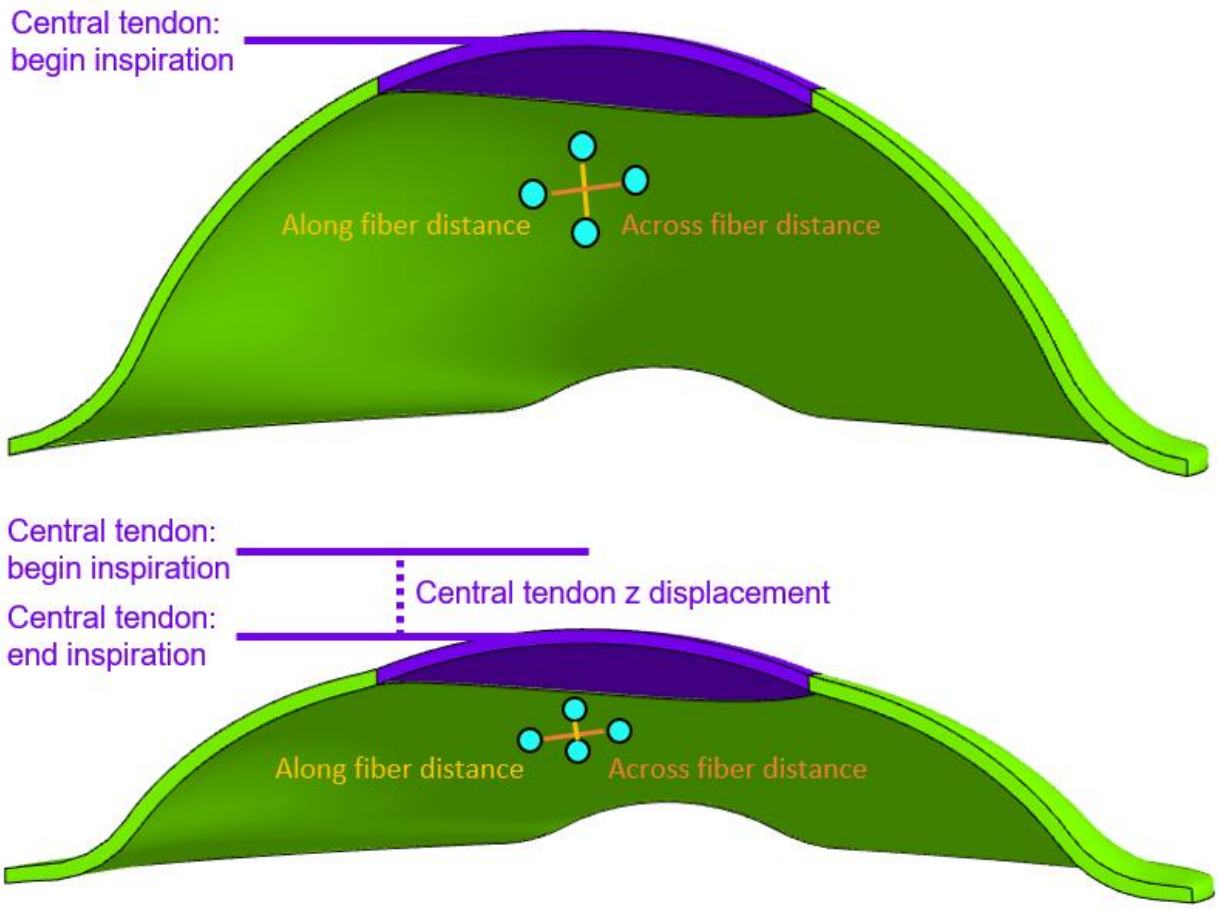

Figure 4.3: Model measurements of diaphragm function

4.4 Results

Inverse finite element simulations were successfully run to fit experimental equibiax passive mechanical testing data from Chapter 2 to the constitutive equation detailed previously (Fig 4.4).

Four simulations were performed corresponding to 6-month-old and 12-month-old wildtype and *mdx* mice and predicted along and across fiber strains were compared to strains measured via sonomicrometry in Chapter 3 (Fig 4.5). Model predictions of 6 and 12-month-old along fiber strains in healthy mice were higher than those measured *in vivo* via sonomicrometry (6mo: model = -0.16, sono = -0.092 ± 0.042; 12mo: model = -0.15, sono = -0.069 ± 0.038). However, cross fiber strains were much lower than those measured *in vivo* (6mo: model =

0.017, sono = 0.119 ± 0.047; 12mo: model = 0.016, sono = 0.039 ± 0.011). In contrast, for *mdx* mice, the model predicted much lower along fiber strains at 6 and 12-months of age (6mo: model = -0.014, sono = -0.028 ± 0.012, 12mo: model = -0.0138, sono = -0.072 ± 0.058). Similar to the wildtype model, predictions of across fiber strains in the *mdx* model were much lower than sonomicrometry measurements at both 6 and 12 months of age (6mo: model = 0.0018, sono = 0.036 ± 0.011; 12mo: model = 0.0015, sono = 0.036 ± 0.016). In addition to comparisons against sonomicrometry strains, model predictions of diaphragm amplitude, superior-inferior displacement, were compared against literature values measured via ultrasound[44] (Fig 4.6). Similar to the predictions of along fiber strains, the model also predicted higher diaphragm displacements for young and aged wildtype mice (young: model = 1.6, ultrasound = 1.14 ± 0.05; aged: model = 1.48, ultrasound = 0.99 ± 0.05). Additionally, model predictions of young and aged *mdx* mice diaphragm amplitude were lower than those measured via ultrasound (young: model = 0.27, ultrasound = 0.83 ± 0.05; aged: model = 0.19, ultrasound = 0.45 ± 0.06).

Simulations of changes to the dystrophic muscle model parameters to those of healthy muscle were performed. Changing only the specific tension (ST) resulted in a recovery of 74.7% of the difference between dystrophic and healthy muscle along fiber strain. For the passive properties, changing only the along fiber properties resulted in 35.2% recovery while changing only the across fiber properties actually caused a further 3% reduction. Finally changing both the along and across fiber passive properties resulted in a 30.6% recovery. (Fig 4.7A) Diaphragm amplitude followed a similar trend where changing the specific tension resulted in a recovery of 73.5%; the along fiber, 33.6%; the across fiber, -4.3%; and both along and across fiber, 30.6% (Fig 4.7B).

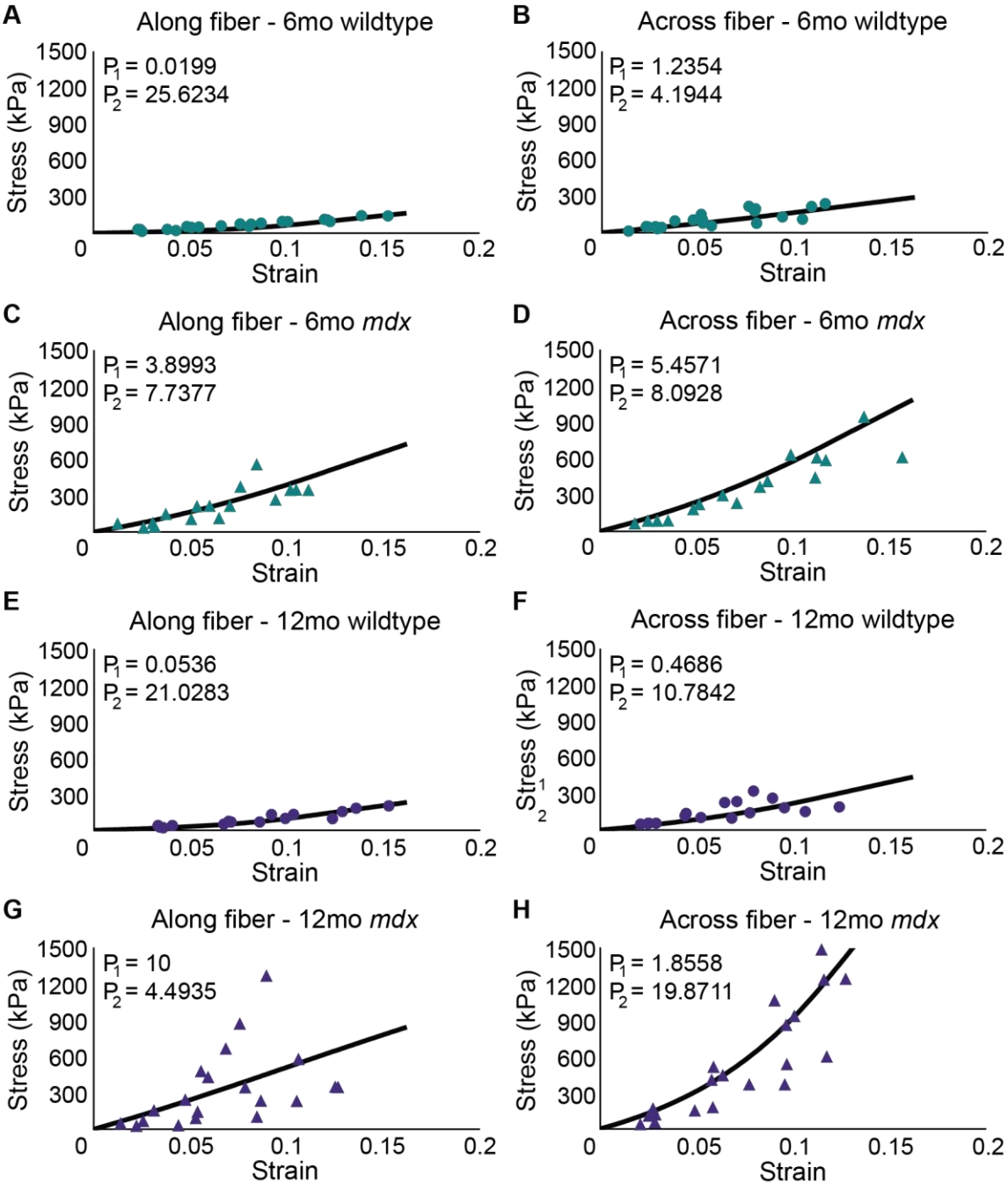

Figure 4.4: Slab model fits to biaxial data from Chapter 2

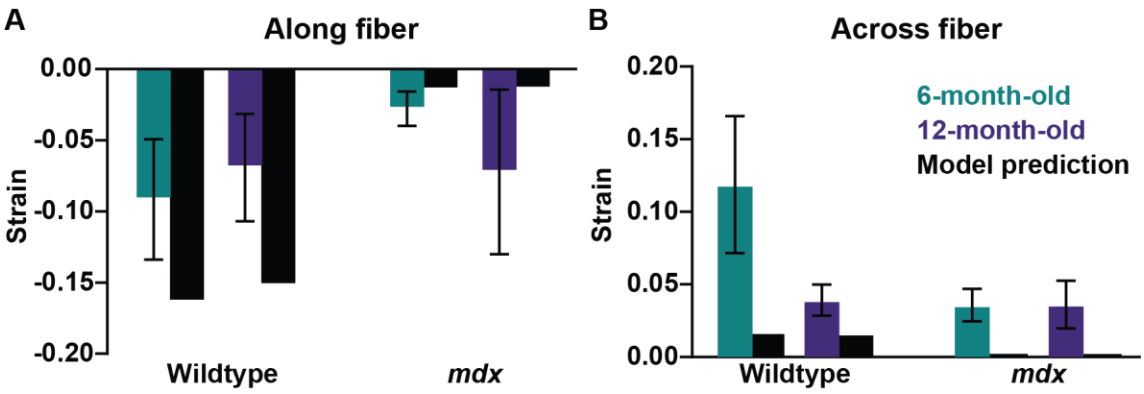

Figure 4.5: Model predictions of (A) along and (B) across fiber strains compared to experimental in vivo strains measured via sonomicrometry

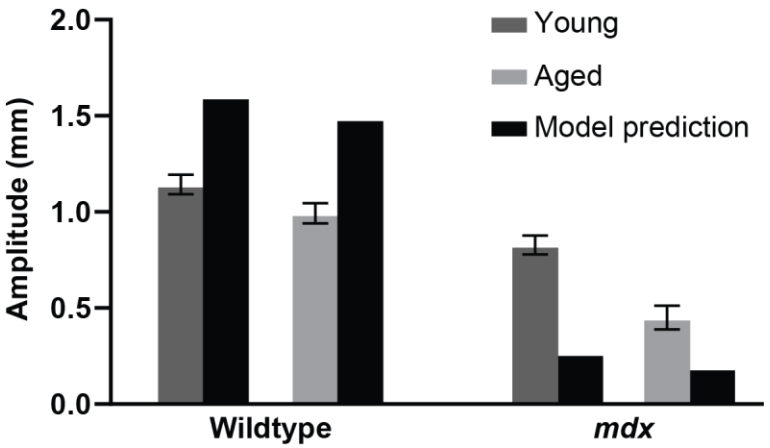

Figure 4.6: Model predictions of diaphragm amplitude, superior-inferior displacement, compared to measurements collected via ultrasound imaging

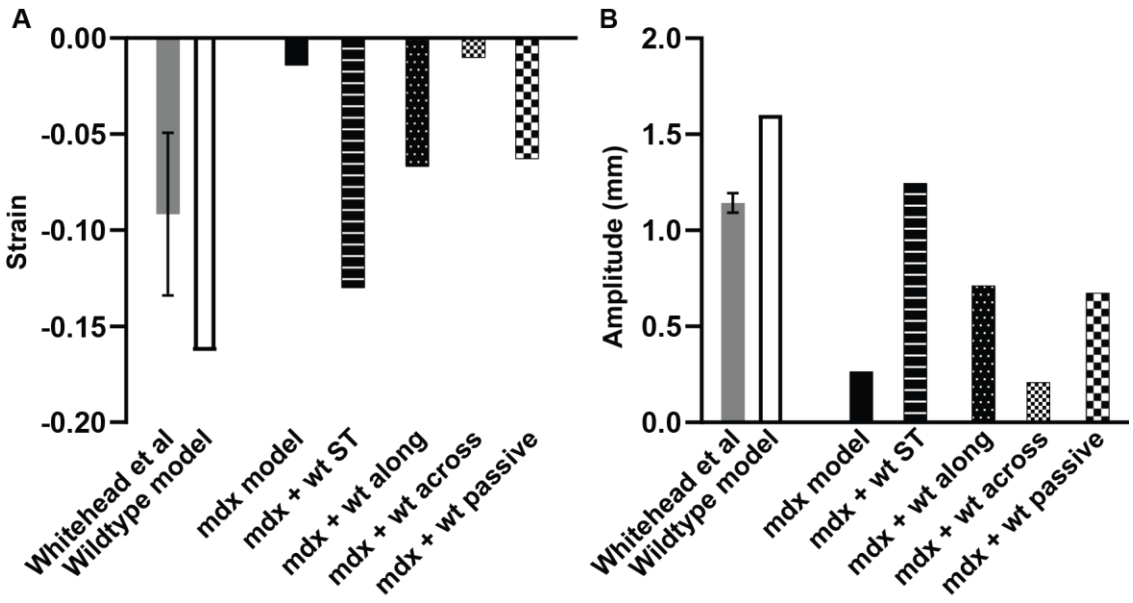

Figure 4.7: Model predictions of (A) along fiber strain and (B) diaphragm amplitude when substituting healthy parameters into the dystrophic model.

4.5 Discussion

The overall goal of this work was to create a finite element model of the mouse diaphragm to investigate the role of active and passive mechanics on diaphragm dysfunction in muscular dystrophy. We segmented publicly available high resolution MR images of a healthy mouse to obtain a 3D model of the diaphragm model. Biaxial mechanical testing data was then fit to a transversely isotropic, hyperelastic, quasi-incompressible material. Finally, simulations were performed comparing changing the active mechanics, specific tension, and the passive mechanics, P_1 and P_2, from the dystrophic values to the healthy values to determine diaphragm function recovery.

Stress strain data from passive biaxial mechanical testing in Chapter 2 were fit to the constitutive equation detailed previously. The passive behavior of this model is defined by a piece-wise exponential function. Due to the nature of exponentials, the number of local minima is expansive and it is possible that we did not determine the global minimum but we are confident in our fits due to the strict convergence tolerance, 0.001, applied to our inverse finite element simulations. Furthermore, predicted strains within the model did not exceed those measured during mechanical testing providing us with more confidence in our parameter optimization.

Our simulations overpredicted along fiber strains and underpredicted across fiber strains for wildtype mice. Conversely, it underpredicted both along and across fiber strains for wildtype mice. We believe that the underprediction of the across fiber strains is due to the mixture model chosen. A transversely isotropic, hyperelastic, quasi-incompressible material is used in both the along fiber and across fiber direction. The third direction is defined by the shear parameter of the previous two materials but this shear parameter affects both off-axis values so it could not simply be increased to the magnitude of the along and across fiber directions. Due to this

direction being significantly less stiff and muscle being an incompressible material, the majority of the deformation occurred in this direction rather than the across fiber. This issue became magnified for the dystrophic muscle which is significantly stiffer than the wildtype causing the across fiber strains to approach zero.

In order to elucidate the individual influences of the changes in passive and active mechanics on diaphragm dysfunction in muscular dystrophy, we investigated how changing dystrophic parameters to their healthy value would affect our measures of diaphragm function. For both along fiber strain and diaphragm amplitude, increasing the specific tension accounted for a recovery of ~74% of the deficit in function. Changing the along fiber passive properties resulted in a ~35% recovery and all passive properties in a ~30% recovery. Drug therapies and treatments are typically focused on active force recovery which is justified by the 74% recovery in function with an increase in force production however the passive properties and increased stiffness of the muscle should also be considered. A 30% recovery in function will not bring respiratory function up to normal levels, however it could delay the need for further assistive respiratory devices.

To conclude, we segmented MR images of a wildtype mouse to build a finite element model of the diaphragm that we then tuned with experimental data from Chapters 2 and previous studies. Output metrics of diaphragm from this model were then compared to *in vivo* strains from Chapter 3 and literature diaphragm amplitude measurements and found to follow similar trends. Finally, we used this model to generate insight into the role of active and passive changes on dystrophic muscle and found that restoring active function results in a 74% recovery while decreasing the passive stiffness to healthy levels results in a 35% recovery. This separation of the different detriments associated with DMD highlights the need to not only consider strengthening muscles, but also controlling the unregulated fibrosis associated with DMD in order to restore diaphragm function.

Chapter 5

Conclusions

5.1 Summary

My goal in this dissertation was to investigate the impact of fibrosis on the active and passive mechanics of the dystrophic diaphragm. Understanding the function and dysfunction of the diaphragm is critical to the care and treatment of boys with DMD because its degeneration ultimately leads to cardiopulmonary failure. Muscle degeneration in DMD is associated with the replacement of contractile tissue with fibrotic tissue and fat. Therapy development is typically aimed towards restoring the dystrophin protein or restoring the contractile tissue but I hypothesized that the fibrotic nature of the disease would also significantly alter the active and passive mechanics.

To quantify the impact of collagen on the passive mechanics of the diaphragm I performed biaxial mechanical tests on healthy and dystrophic diaphragm muscle tissue samples before and after collagen digestion. These measurements revealed a significant relationship between the amount of collagen and both the along and across fiber stiffness. Sonometric measurements of *in vivo* diaphragm contraction revealed decreased strains in both the along and across fiber directions. Experimental data from my two mouse model experiments were used to inform a finite element model of the diaphragm. Model predictions were used to evaluate how substituting healthy active and passive mechanics would improve dystrophic diaphragm function and found a 74% recovery with active mechanics and a 35% recovery with passive.

Overall, this experimental-modeling coupled framework provided insight into both the active and passive mechanics of the diaphragm and how those are altered by the fibrotic nature of DMD. Moving forward, the experimental methods utilized in this dissertation could provide

additional testing metrics for future drug therapies. Further development of the finite element model could also make it a viable tool for identifying targets for treatment.

5.2 Contributions

Biaxial measurements of dystrophic diaphragm

Previous studies have been performed measuring the passive mechanics of dystrophic diaphragm muscle tissue[5,9,10,19] however all of these studies were conducted on strips of muscle in the fiber direction only. The unique architecture of the diaphragm and the fact that its only truly unconstrained in one direction lends itself to biaxial testing and studies on healthy diaphragm tissue have emphasized this.[21,22]

In this work, I have contributed the first passive biaxial mechanical testing data of *mdx* mouse muscle to our knowledge. The diaphragm is known to be constrained in the along and across fiber directions and these additional constraints will alter the force response of the muscle compared to a muscle only constrained in one direction. Additionally, the across fiber direction is important to characterize in relation to DMD as collagen laid down as a result of the inflammatory response will not have the same orientation as collagen from healthy tissue. The orientation of the collagen within the tissue will affect the passive mechanics.

Impact of collagen on passive mechanics

One goal of this work was to investigate the impact of collagen on the passive mechanics of the diaphragm as prior to this work, their relationship remained unclear. To accomplish this, I performed biaxial passive tests on wildtype and *mdx* diaphragm muscle tissue samples before and after enzymatic collagen digestion. This protocol allowed for paired comparisons between samples before and after treatment to isolate the impact of collagen on the measured force response. My results revealed a significant decrease in the stiffness of dystrophic muscle following digestion of collagen that coincided with a significant decrease in collagen quantity as measured by picrosirius red staining. Furthermore, a linear regression between muscle stiffness

and collagen area fraction confirmed the relationship between collagen quantity and muscle stiffness in both the along and across fiber direction.

***In vivo* along and across fiber strain measurements**

In vivo assessments of dystrophic diaphragm function have been limited to indirect measurements through respiration and imaging techniques such as MRI and ultrasound. The previously mentioned techniques are unable to capture the tissue mechanics other than overall displacements. As previously mentioned, studying both the along and across fiber mechanics of the diaphragm is necessary as the two are coupled and differentially affected in diseases such as DMD. Sonomicrometry has been previously used to measure along fiber strains in the much larger dog diaphragm. Using much smaller crystals and gluing instead of sewing the crystals, I was able to adapt this method for use in mice and to measure across fiber strains. Across fiber strains were my next addition by incorporating a second pair of crystals perpendicular to the muscle fiber direction. This experimental method provided new insight to the mechanics of the diaphragm as well as provides a new testing metric for therapies in the *mdx* mouse.

Impact of collagen on active mechanics

My method of measuring both the along and across fiber *in vivo* mechanics of the mouse diaphragm allowed us to next probe the impact of collagen on active mechanics. The *mdx* mouse is known to replicate the DMD phenotype in its diaphragm including the increase in collagen quantity. Collagen amount was measured by imaging picrosirius red stained sections confirming significantly higher quantities in *mdx* mice compared to wildtype. Measured *in vivo* along and across fiber strains were significantly correlated with collagen area fraction where an increase in collagen results in a decrease in measured strains.

Impact of active and passive mechanics on the dystrophic diaphragm

My thesis work has added to our understanding of how collagen impacts both the active and passive mechanics in the diaphragm. How these mechanics individually contribute to the dysfunction of the diaphragm is unknown. Computational models allow for us to gain insight into

questions like this by performing simulations that would be difficult to impossible with standard experiments. With my computational model, I was able to probe the active and passive mechanics separately by changing the parameters of each independently. Model predictions determined that there was roughly a 70/30 split in ability to restore function to the dystrophic diaphragm between the active and passive mechanics, respectively.

5.3 Future applications

The goal of this work was to conduct experiments to probe the role of collagen in diaphragm dysfunction in DMD and then use this data to inform a computational model that could predict how changes in collagen would affect diaphragm function. The work presented in this dissertation has highlighted the need to consider collagen and its impact on muscle function in the care of boys with DMD. Next steps in this work would include repeating passive testing protocols with the strains measured in our sonomicrometry experiments, including additional crystals in the sonomicrometry experiments to investigate regional differences as well as boundary conditions, and further development and tuning of the computational model to better match experimental findings.

Similar to previous work in the healthy diaphragm, we believed that equibiaxial protocols were the most representative of the *in vivo* stretches of the diaphragm. While our protocol was adequate for measuring the impact of collagen on the passive properties of the diaphragm, we believe future studies should attempt to match the strains measured *in vivo*. In addition to being more physiologically accurate, the stiffnesses calculated from stresses measured this way may better explain the differences in strains measured via sonomicrometry.

Our sonomicrometry study built upon previous methods by incorporating the across fiber direction as well. Future work could build further upon this by measuring strains in different regions of the diaphragm as previous studies have shown regional variability in other metrics of muscle function.[44,47] Additionally, measurements of the displacement of the attachment to the

ribs should be collected. Studies on boys with DMD have revealed morphologic changes to the structure of the ribs[48] and it is reasonable to expect that similar changes would occur in *mdx* mice. These measurements would also assist in the improvement of the finite element model.

The finite element model of the mouse diaphragm was insightful in its predictions of recovery associated with restoration of healthy active and passive properties. Next steps in the model would be further tuning of the material properties to better match the experimental data. One possible way to do this would be by altering the specific tension, current values are incorporated from the literature but tend to have a large variability. The boundary conditions of the model could also be improved. Currently the ribs are fixed from translating inferiorly/superiorly however this is not physiologically accurate. Unfortunately, we did not have the necessary data to determine the correct movement of the ribs but the previously suggested sonomicrometry experiment or higher resolution MR scans could potentially provide this insight.

5.4 Final remarks

In DMD, the chronic state of inflammation leads to contractile tissue in muscle being replaced by fibrotic tissue and fat, affecting both the active and passive mechanics of the muscle. I hypothesized that the increased collagen would be a significant source of the altered mechanics associated with dystrophic muscle. In this dissertation, I coupled novel experiments and computational modeling to isolate the impact of collagen on the active and passive mechanics of the diaphragm and performed “what-if” simulations to understand how recovery of each affects diaphragm function. Overall, we found that collagen significantly impacts both the active and passive mechanics and that both are able to partially restore diaphragm function highlighting the need to further study collagen’s role in DMD.

References

1. Straub V, Rafael JA, Chamberlain JS, Campbell KP. Animal Models for Muscular Dystrophy Show Different Patterns of Sarcolemmal Disruption. *J Cell Biol*. 1997;139(2):375-385.

2. García-Pelagio KP, Bloch RJ, Ortega A, González-Serratos H. Biomechanics of the sarcolemma and costameres in single skeletal muscle fibers from normal and dystrophin-null mice. *J Muscle Res Cell Motil*. 2011;31(0):323-336. doi:10.1007/s10974-011-9238-9

3. Rosenberg AS, Puig M, Nagaraju K, et al. Immune-mediated pathology in Duchenne muscular dystrophy. *Sci Transl Med*. 2015;7(299):299rv4. doi:10.1126/scitranslmed.aaa7322

4. Emery AEH. The muscular dystrophies. *BMJ*. 1998;317(7164):991-995.

5. Bates G, Sigurdardottir S, Kachmar L, et al. Molecular, cellular, and muscle strip mechanics of the *mdx* mouse diaphragm. *American Journal of Physiology-Cell Physiology*. 2013;304(9):C873-C880. doi:10.1152/ajpcell.00220.2012

6. Capogrosso RF, Mantuano P, Cozzoli A, et al. Contractile efficiency of dystrophic mdx mouse muscle: in vivo and ex vivo assessment of adaptation to exercise of functional end points. *Journal of Applied Physiology*. 2017;122(4):828-843. doi:10.1152/japplphysiol.00776.2015

7. Chan S, Head SI, Morley JW. Branched fibers in dystrophic *mdx* muscle are associated with a loss of force following lengthening contractions. *American Journal of Physiology-Cell Physiology*. 2007;293(3):C985-C992. doi:10.1152/ajpcell.00128.2007

8. Watchko JF, O'Day TL, Hoffman EP. Functional characteristics of dystrophic skeletal muscle: insights from animal models. *Journal of Applied Physiology*. 2002;93(2):407-417. doi:10.1152/japplphysiol.01242.2001

9. Stedman HH, Sweeney HL, Shrager JB, et al. The mdx mouse diaphragm reproduces the degenerative changes of Duchenne muscular dystrophy. *Nature*. 1991;352(6335):536-539. doi:10.1038/352536a0

10. Smith LR, Barton ER. Collagen content does not alter the passive mechanical properties of fibrotic skeletal muscle in *mdx* mice. *American Journal of Physiology-Cell Physiology*. 2014;306(10):C889-C898. doi:10.1152/ajpcell.00383.2013

11. Bushby K, Finkel R, Birnkrant DJ, et al. Diagnosis and management of Duchenne muscular dystrophy, part 2: implementation of multidisciplinary care. *The Lancet Neurology*. 2010;9(2):177-189. doi:10.1016/S1474-4422(09)70272-8

12. Birnkrant DJ, Bushby K, Bann CM, et al. Diagnosis and management of Duchenne muscular dystrophy, part 2: respiratory, cardiac, bone health, and orthopaedic management. *Lancet Neurol*. 2018;17(4):347-361. doi:10.1016/S1474-4422(18)30025-5

13. Buyse GM, Rummey C, Meier T, et al. Home-Based Monitoring of Pulmonary Function in Patients with Duchenne Muscular Dystroph. *J Neuromuscul Dis*. 5(4):419-430. doi:10.3233/JND-180338

14. Pennati F, Arrigoni F, LoMauro A, et al. Diaphragm Involvement in Duchenne Muscular Dystrophy (DMD): An MRI Study. *Journal of Magnetic Resonance Imaging*. 2020;51(2):461-471. doi:10.1002/jmri.26864

15. Rowe J, Chen Q, Domire ZJ, et al. Effect of collagen digestion on the passive elastic properties of diaphragm muscle in rat. *Medical Engineering & Physics*. 2010;32(1):90-94. doi:10.1016/j.medengphy.2009.11.002

16. Blemker SS, Pinsky PM, Delp SL. A 3D model of muscle reveals the causes of nonuniform strains in the biceps brachii. *Journal of Biomechanics*. 2005;38(4):657-665. doi:10.1016/j.jbiomech.2004.04.009

17. Hoffman EP, Brown RH, Kunkel LM. Dystrophin: The Protein Product of the Duchenne Muscular Dystrophy Locus. :10.

18. Emery AEH. Population frequencies of inherited neuromuscular diseases—A world survey. *Neuromuscular Disorders*. 1991;1(1):19-29. doi:10.1016/0960-8966(91)90039-U

19. Dupont-Versteegden EE, McCarter RJ. Differential expression of muscular dystrophy in diaphragm versus hindlimb muscles of mdx mice. *Muscle Nerve*. 1992;15(10):1105-1110. doi:10.1002/mus.880151008

20. Boriek AM, Zhu D, Zeller M, Rodarte JR. Inferences on force transmission from muscle fiber architecture of the canine diaphragm. :10.

21. Boriek AM, Kelly NG, Rodarte JR, Wilson TA. Biaxial constitutive relations for the passive canine diaphragm. *Journal of applied physiology*. 2000;89(6):2187-2190.

22. Boriek AM, Rodarte JR, Reid MB. Shape and tension distribution of the passive rat diaphragm. *Am J Physiol Regulatory Integrative Comp Physiol*. 2001;280:33-41.

23. Anderson BR, Granzier HL. Titin-based tension in the cardiac sarcomere: molecular origin and physiological adaptations. *Prog Biophys Mol Biol*. 2012;110(2-3):204-217. doi:10.1016/j.pbiomolbio.2012.08.003

24. Chung CS, Granzier HL. Contribution of titin and extracellular matrix to passive pressure and measurement of sarcomere length in the mouse left ventricle. *J Mol Cell Cardiol*. 2011;50(4):731-739. doi:10.1016/j.yjmcc.2011.01.005

25. Manning J, Buckley MM, O'Halloran KD, O'Malley D. Combined XIL-6R and urocortin-2 treatment restores MDX diaphragm muscle force. *Muscle & Nerve*. 2017;56(6):E134-E140. doi:10.1002/mus.25644

26. Fomovsky GM, Holmes JW. Evolution of scar structure, mechanics, and ventricular function after myocardial infarction in the rat. *American Journal of Physiology-Heart and Circulatory Physiology*. 2010;298(1):H221-H228. doi:10.1152/ajpheart.00495.2009

27. Rushmer RF, Franklin DL, Ellis RM. Left Ventricular Dimensions Recorded by Sonocardiometry. *Circulation Research*. 1956;4(6):684-688. doi:10.1161/01.RES.4.6.684

28. Newman S, Road J, Bellemare F, Clozel JP, Lavigne CM, Grassino A. Respiratory muscle length measured by sonomicrometry.

29. Road J, Newman S, Derenne JP, Grassino A. In vivo length-force relationship of canine diaphragm. *Journal of Applied Physiology*. 1986;60(1):63-70.

30. Sassoon CS, Zhu E, Fang L, Sieck GC, Powers SK. Positive end-expiratory airway pressure does not aggravate ventilator-induced diaphragmatic dysfunction in rabbits. *Crit Care*. 2014;18(5). doi:10.1186/s13054-014-0494-0

31. Zajac FE. Muscle and tendon: properties, models, scaling, and application to biomechanics and motor control. *Crit Rev Biomed Eng*. 1989;17(4):359-411.

32. Fiorentino NM, Blemker SS. Musculotendon variability influences tissue strains experienced by the biceps femoris long head muscle during high-speed running. *J Biomech*. 2014;47(13):3325-3333. doi:10.1016/j.jbiomech.2014.08.010

33. Rehorn MR, Blemker SS. THE EFFECTS OF APONEUROSIS GEOMETRY ON STRAIN INJURY SUSCEPTIBILITY EXPLORED WITH A 3D MUSCLE MODEL. *J Biomech*. 2010;43(13):2574-2581. doi:10.1016/j.jbiomech.2010.05.011

34. Pelland CM, Feng X, Borowitz KC, Meyer CH, Blemker SS. A Dynamic Magnetic Resonance Imaging–Based Method to Examine In Vivo Levator Veli Palatini Muscle Function During Speech. *J Speech Lang Hear Res*. 2019;62(8):2713-2722. doi:10.1044/2019_JSLHR-S-18-0459

35. Rahimov F, Kunkel LM. Cellular and molecular mechanisms underlying muscular dystrophy. *Journal of Cell Biology*. 2013;201(4):499-510. doi:10.1083/jcb.201212142

36. Chapman MA, Zhang J, Banerjee I, et al. Disruption of both nesprin 1 and desmin results in nuclear anchorage defects and fibrosis in skeletal muscle. *Human Molecular Genetics*. 2014;23(22):5879-5892. doi:10.1093/hmg/ddu310

37. Eilaghi A, Flanagan JG, Brodland GW, Ethier CR. Strain Uniformity in Biaxial Specimens is Highly Sensitive to Attachment Details. *Journal of Biomechanical Engineering*. 2009;131(9):091003. doi:10.1115/1.3148467

38. Bromage TG, Goldman HM, McFarlin SC, Warshaw J, Boyde A, Riggs CM. Circularly polarized light standards for investigations of collagen fiber orientation in bone. *The Anatomical Record*. 2003;274B(1):157-168. doi:10.1002/ar.b.10031

39. Rich L, Whittaker P. Collagen and picrosirius red staining: a polarized light assessment of fibrillar hue and spatial distribution. *Braz J Morphol Sci*. 2005;22(2):97-104.

40. Raghupathy R, Barocas V. *Robust Image Correlation Based Strain Calculator for Tissue Systems*. http://license.umn.edu/technologies/20130022_robust-image-correlation-based-strain-calculator-for-tissue-systems

41. Caggiano LR, Lee JJ, Holmes JW. Surgical reinforcement alters collagen alignment and turnover in healing myocardial infarcts. *Am J Physiol Heart Circ Physiol*. 2018;315(4):H1041-H1050. doi:10.1152/ajpheart.00088.2018

42. Granzier HL, Irving TC. Passive tension in cardiac muscle: contribution of collagen, titin, microtubules, and intermediate filaments. *Biophys J*. 1995;68(3):1027-1044.

43. Boriek AM, Miller CC, Rodarte JR. Muscle fiber architecture of the dog diaphragm. *Journal of Applied Physiology*. 1998;84(1):318-326. doi:10.1152/jappl.1998.84.1.318

44. Whitehead NP, Bible KL, Kim MJ, Odom GL, Adams ME, Froehner SC. Validation of ultrasonography for non-invasive assessment of diaphragm function in muscular dystrophy. *J Physiol*. 2016;594(24):7215-7227. doi:10.1113/JP272707

45. Daley MA, Voloshina A, Biewener AA. The role of intrinsic muscle mechanics in the neuromuscular control of stable running in the guinea fowl. *J Physiol*. 2009;587(Pt 11):2693-2707. doi:10.1113/jphysiol.2009.171017

46. Azizi E. Locomotor function shapes the passive mechanical properties and operating lengths of muscle. *Proc Biol Sci*. 2014;281(1783). doi:10.1098/rspb.2013.2914

47. Henry CC, Martin KS, Ward BB, Handsfield GG, Peirce SM, Blemker SS. Spatial and age-related changes in the microstructure of dystrophic and healthy diaphragms. *PLoS One*. 2017;12(9). doi:10.1371/journal.pone.0183853

48. Barnard AM, Lott DJ, Batra A, et al. Imaging respiratory muscle quality and function in Duchenne muscular dystrophy. *J Neurol*. 2019;266(11):2752-2763. doi:10.1007/s00415-019-09481-z

49. Porter JD. A chronic inflammatory response dominates the skeletal muscle molecular signature in dystrophin-deficient mdx mice. *Human Molecular Genetics*. 2002;11(3):263-272. doi:10.1093/hmg/11.3.263

50. Johnson GA, Cofer GP, Gewalt SL, Hedlund LW. Morphologic Phenotyping with MR Microscopy: The Visible Mouse. *Radiology*. 2002;222(3):789-793. doi:10.1148/radiol.2223010531

51. Handsfield GG, Meyer CH, Hart JM, Abel MF, Blemker SS. Relationships of 35 lower limb muscles to height and body mass quantified using MRI. *Journal of Biomechanics*. 2014;47(3):631-638. doi:10.1016/j.jbiomech.2013.12.002

52. Handsfield GG, Bolsterlee B, Inouye JM, Herbert RD, Besier TF, Fernandez JW. Determining skeletal muscle architecture with Laplacian simulations: a comparison with diffusion tensor imaging. *Biomech Model Mechanobiol*. 2017;16(6):1845-1855. doi:10.1007/s10237-017-0923-5

53. Maas SA, Ellis BJ, Ateshian GA, Weiss JA. FEBio: Finite Elements for Biomechanics. *J Biomech Eng*. 2012;134(1):11005-NaN. doi:10.1115/1.4005694

54. Greising SM, Sieck DC, Sieck GC, Mantilla CB. Novel method for transdiaphragmatic pressure measurements in mice. *Respir Physiol Neurobiol*. 2013;188(1):56-59. doi:10.1016/j.resp.2013.04.018

Appendix A: Passive biaxial mechanical testing protocol development

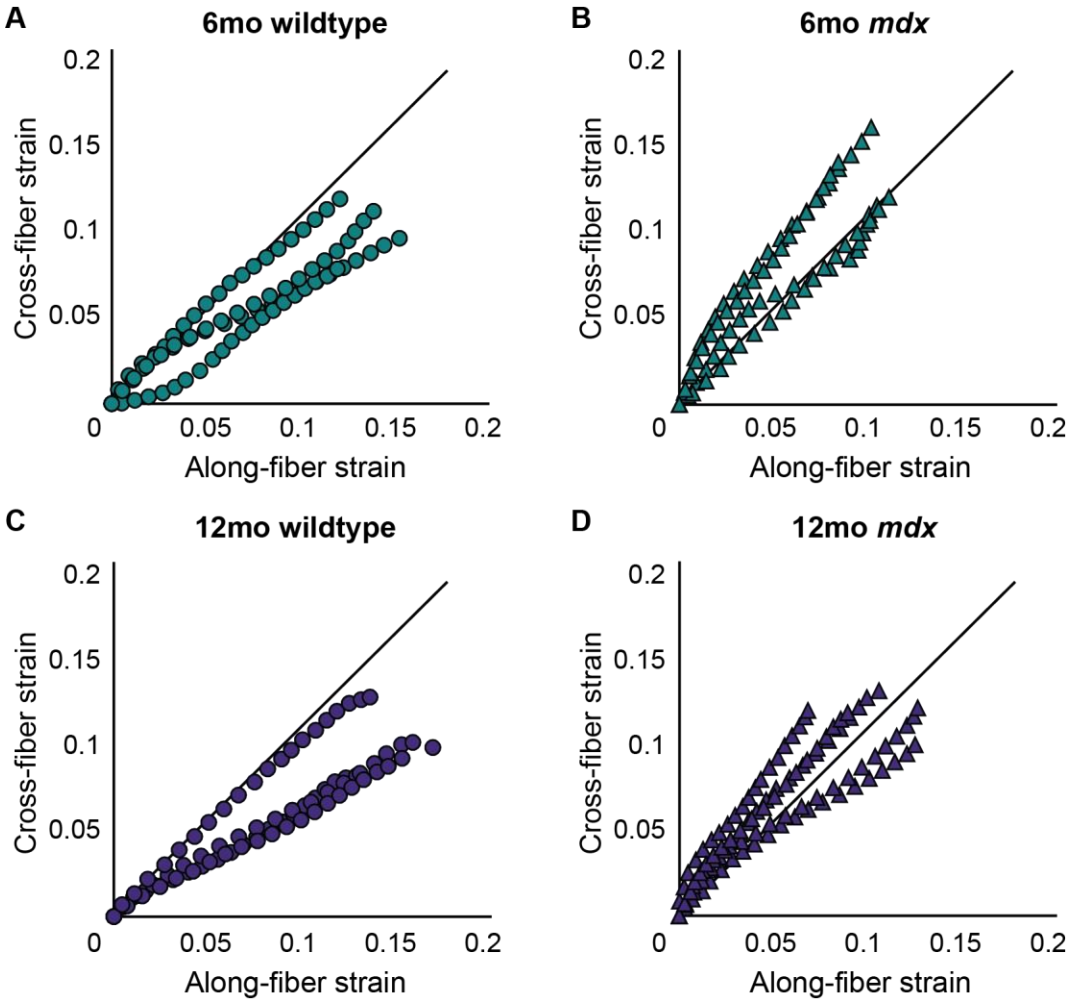

Figure A1: Strain calculations from digital image correlation in the along-fiber and cross-fiber directions for (A) 6-month-old wildtype (B) 6-month-old *mdx* (C) 12-month-old wildtype and (D) 12-month-old *mdx* mice.

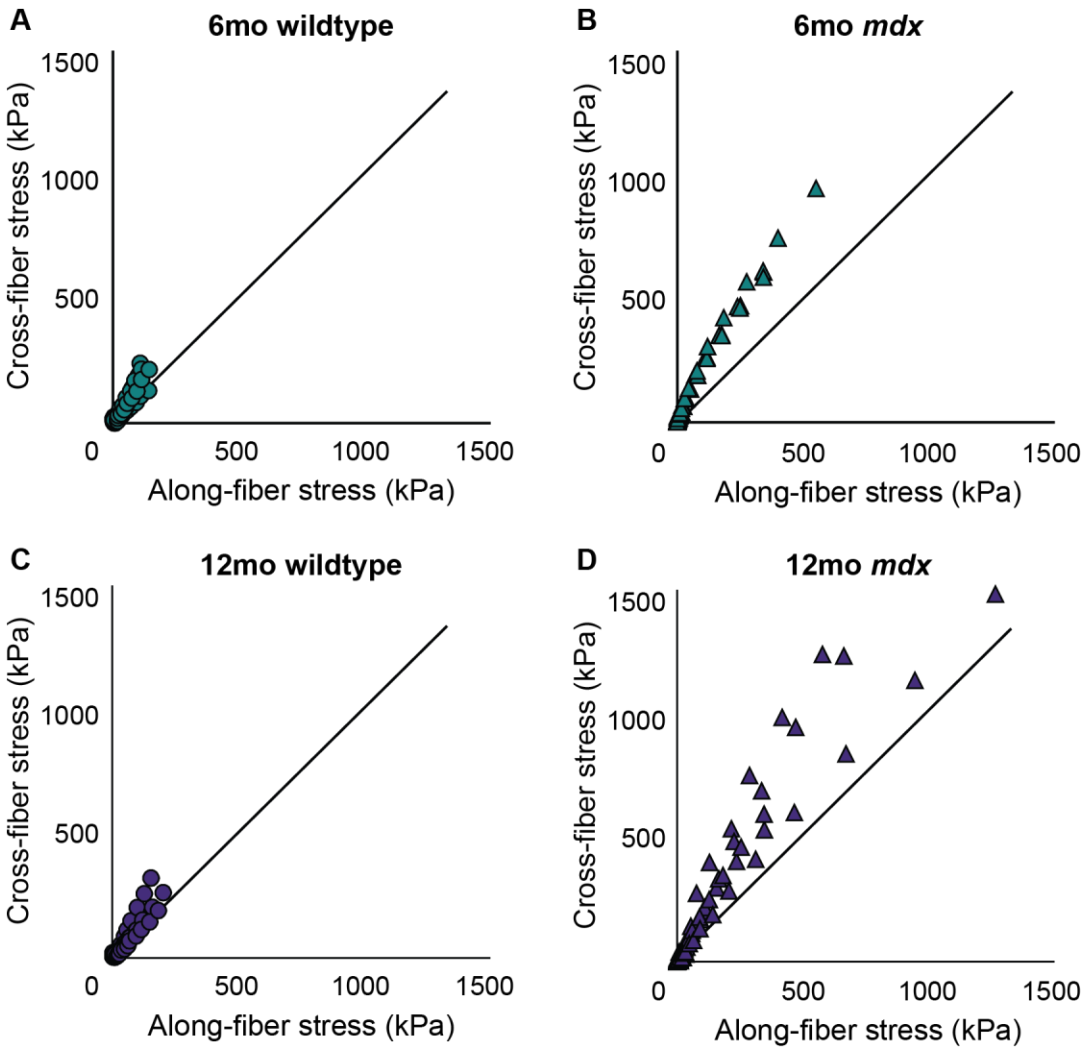

Figure A2: Calculated along-fiber and cross-fiber stress from the final prescribed 20% rake strain run for (A) 6-month-old wildtype (B) 6-month-old *mdx* (C) 12-month-old wildtype and (D) 12-month-old *mdx*

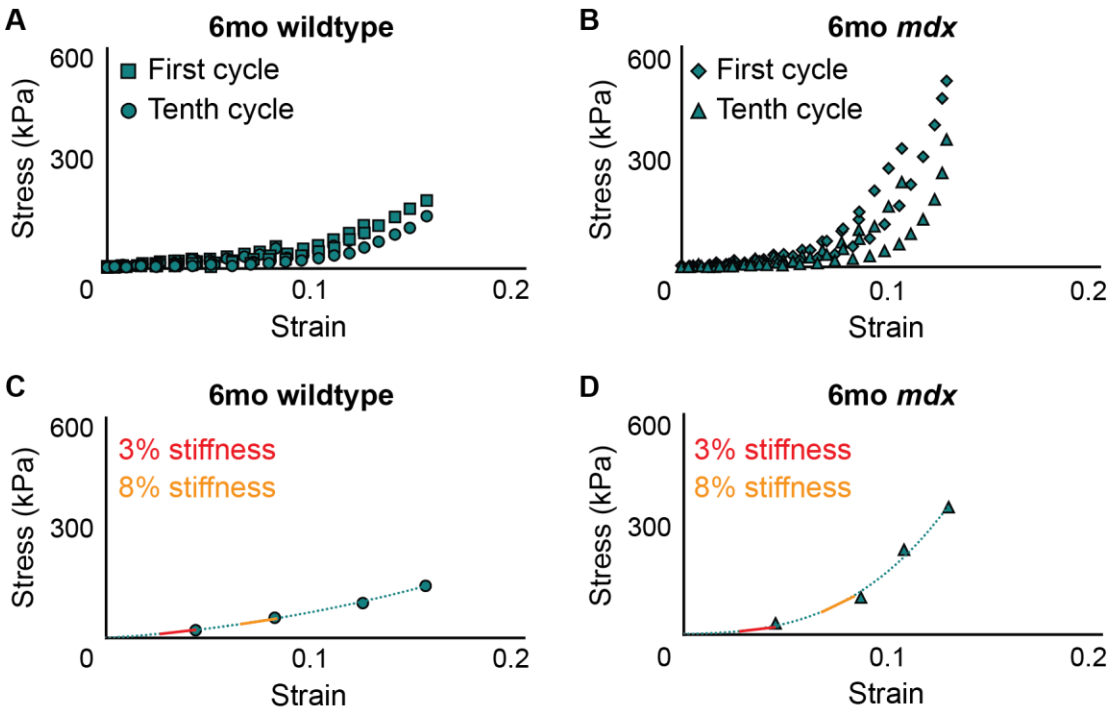

Figure A3: Representative first and tenth (final) stress strain curves for (A) 6-month-old wildtype and (B) 6-month-old *mdx* mice. At each prescribed rake strain, hysteresis occurs during the ten cycles resulting in a stress softening effect however the first cycle of each higher strain following the tenth cycle of the previous strain shows that samples are not being damaged. (C, D) The quasi-static behavior for each sample was obtained by taking the final point from each prescribed rake strain. Instantaneous slopes were calculated at 3 and 8% strain to calculate the stiffness of each sample.